Cardiac Left Atrium and Left Ventricle Segmentation in 3D MRI

Author

Ibtihaj Ahmad

Registration Number

170607

Supervisor

Dr.Farhan Hussain

DEPARTMENT OF COMPUTER AND SOFTWARE ENGINEERING

COLLEGE OF ELECTRICAL AND MECHANICAL ENGINEERING

NATIONAL UNIVERSITY OF SCIENCES AND TECHNOLOGY

ISLAMABAD

JANUARY, 2019

Cardiac Left Atrium and Left Ventricle Segmentation in 3D MRI

Author

Ibtihaj Ahmad

Registration Number

170607

A thesis submitted in partial fulfillment of the requirements for the degree of

MS Computer Engineering

Thesis Supervisor:

Dr.Farhan Hussain

Thesis Supervisor's Signature: ____

DEPARTMENT OF COMPUTER AND SOFTWARE ENGINEERING

COLLEGE OF ELECTRICAL AND MECHANICAL ENGINEERING

NATIONAL UNIVERSITY OF SCIENCES AND TECHNOLOGY

ISLAMABAD

JANUARY, 2019

Declaration

I certify that this research work titled "*Cardiac Left Atrium and Left Ventricle Segmentation in 3D MRI*" is my own work. The work has not been presented elsewhere for assessment. The material that has been used from other sources it has been properly acknowledged / referred.

Signature of Student

Ibtihaj Ahmad

2016-NUST-Ms-CE-00000170607

Plagiarism Certificate (Turnitin Report)

This thesis has been checked for Plagiarism. Turnitin report endorsed by Supervisor is attached.

Signature of Student

Ibtihaj Ahmad

Registration Number

00000170607

Signature of Supervisor

Copyright Statement

Acknowledgements

I am thankful to my Creator Allah Subhana-Watala to have guided me throughout this work at every step and for every new thought which You setup in my mind to improve it. Indeed I could have done nothing without Your priceless help and guidance. Whosoever helped me throughout the course of my thesis, whether my parents or any other individual was Your will, so indeed none be worthy of praise but You.

I am profusely thankful to my beloved parents who raised me when I was not capable of walking and continued to support me throughout in every department of my life.

I would also like to express special thanks to my supervisor Dr.Farhan Hussain for his help throughout my thesis and also for Machine Learning which he has taught me during master coursework. I can safely say that I haven't learned any other engineering subject in such depth than the ones which he has taught.

I would also like to pay special thanks to Dr.Usman Akram and Dr.Shoab Ahmad Khan for his tremendous support and cooperation. Each time I got stuck in something, he came up with the solution. Without his help I wouldn’t have been able to complete my thesis. I appreciate his patience and guidance throughout the whole thesis.

I would also like to thank Dr.Arslan Shokat and Dr.Wasi Haider Butt for being on my thesis guidance and evaluation committee.

Finally, I would like to express my gratitude to all the individuals especially Fahim Ullah who have rendered valuable assistance to my study.

Dedicated to my exceptional parents whose tremendous support and cooperation led me to this wonderful accomplishment.

Abstract

3D Cardiac Magnetic Resonance Imaging (MRI) is widely used for the diagnosis of cardiac diseases such as congenital heart defect, left ventricular hypertrophy and left atrium hypertrophy etc. It is one of the noninvasive technique to examine cardiac anatomy. However this technique is semi- automatic, i.e. the images obtained directly from MRI machine have to be segmented manually. This includes the segmentation of chambers and vessels, which is quite complex and requires specialized technical knowledge. Without proper segmentation, it is extremely difficult for medical staff to examine the data. This research suggest a fully automatic method for cardiac chamber segmentation (Left Atrium and Left Ventricle pair) in 3D cardiac MRI based on a combination of traditional and artificial intelligence method. The proposed method identifies the junction of Left Atrium (LA) and Left Ventricle (LV) using neural networks. The features used for this purpose are based on shape, size and position. Then it uses traditional methods to track and stack the upper and lower slices based on neighborhood. I.e. a 3D model of the segmented LA and LV is reconstructed from the 2D slices. This enhanced 3D image model helps in deducing quality information for the diagnosis of various heart diseases. The proposed algorithm shows acceptable performances for all planes of LV and LA. We have achieved 91.57% mean segmentation accuracy. The proposed algorithm is not effected by the thickness of the slices. It is simple and computationally less intensive than existing algorithms. The proposed method is applicable to the high resolution (0.5mm) 3D MRI setup. For such high resolution the existing algorithms are not able to perform well.

Key Words: *Cardiac MRI Segmentation, Left Ventricle Segmentation, Left Atrium Segmentation, Heart Chamber Segmentation*

Table of Contents

List of Figures

List of Tables

List of Acronyms Used in the Document.

Acronym Used	**Definition**
ACPS	Adaptive Control Point Status
ASM	Active Shape Model
CC	Coronary Catheterization
DC	Dice Coefficient
FFD	Free Form Deformation
GMM	Gaussian Mixed Model
LA	Left Atrium
LAD	Left Anterior Descending
LARM	Locally Affine Registration Method
LCA	Left Coronary Artery
LV	Left Ventricle
MLP	Maximum Likelihood Probability
MRI	Magnetic Resonance Imaging
MSA	Mean Segmentation Accuracy
PCA	Principal Components Analysis
PDM	Point Distribution Model
RCA	Right Coronary Artery
RA	Right Atrium
RV	Right Ventricle
SSDM	Subject Specific Dynamic Model
SSM	Statistical Shape Model

Chapter 1 : Introduction

The research work in this document is divided into four basic parts i.e. introduction, literature review, proposed method and experimentation setup along with results. Each part is explained in detail in the respective chapters. This chapter give a brief overview of some of the preliminary background, which include

- Basics of MRI,
- Basic cardiac anatomy,
- Background, scope and motivation of the research topic.

1.1 Basics of MRI

A human body is composed of 70% of water. A water molecule possess a hydrogen atom along with a proton. Magnetic Resonance Imaging (MRI) is based on magnetic resonance of these hydrogen protons. These protons are excited when a radio frequency pulse is introduced. When the pulse is removed the protons go back to their relaxation state and releases the energy. The magnetic resonance machine captures the released signals. During relaxation two processes take place i.e. longitudinal relaxation (T1) and transversal relaxation (T2). T1 provides information about anatomy in Z-plane while T2 provides information about anatomy in XY plane.

A human body possess different types of tissues. Each tissue has different proportion of water and fat. Both have different relaxation time (T1 and T2). This create high signal intensity in case of fats and low signal intensity in case of water. With the help of these differences, an image is created.

A 3D MRI possess various slices of single plane (Figure 1.1). This plane may be either axial (transversal), coronel or sagittal. These slices are also known as sequences. Axial plane consist of transversal slices (Figure 1.2). Sagittal plane also known as longitudinal plane, divides the body into right and left parts. Coronal plane is a vertical plane at right angles to a sagittal plane, dividing the body into anterior and posterior portions. Figure 1.2 shows all cross sectional planes i.e. axial, coronal and sagittal.

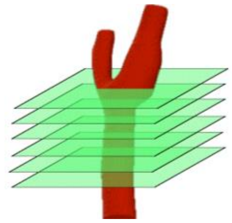

Figure 1.1: Cross sectional axial slices of an artery.

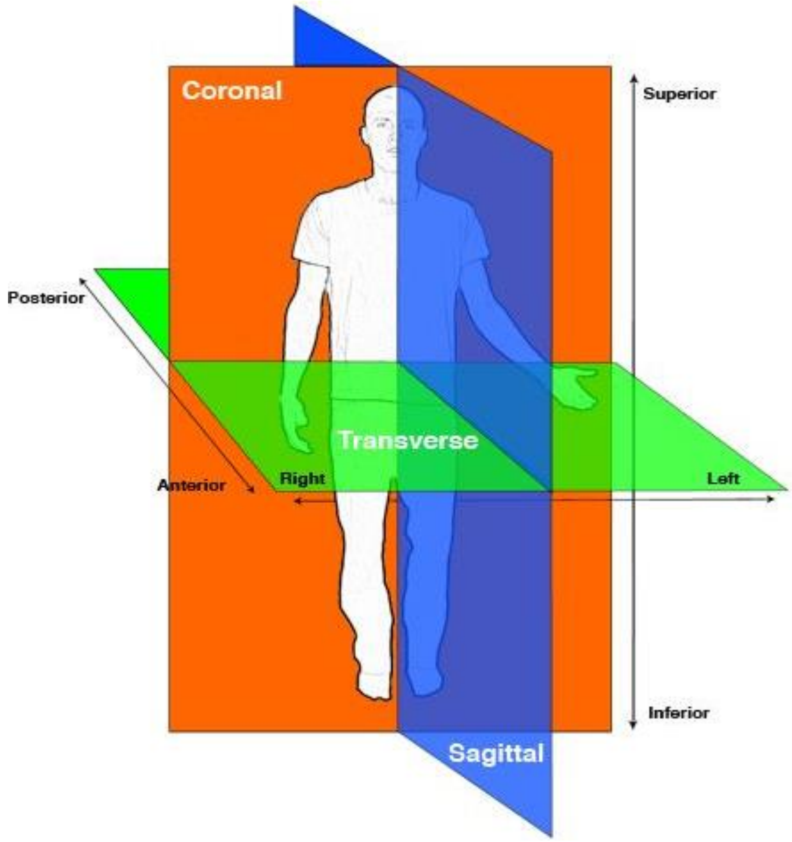

Figure 1.2: MRI planes, axial (transversal), coronal and sagittal [52]

1.2 Basic Cardiac Anatomy in MRI

A human heart can be divided into four chambers, i.e. left atrium (LA), left ventricle (LV), right atrium (RA) and right ventricle (RV). Figure 1.3 shows all the respective cardiac chambers while figure 1.4 shows all the respective chambers in an axial slice. In MRI slices the color of LA and LV is light gray, this is due to the fact that these chamber possesses more pool of blood. RA and RV is light gray due to lesser blood pool. It can be observed from Figure 1.4 that in an MRI the LA and LV shape resembles an ellipse.

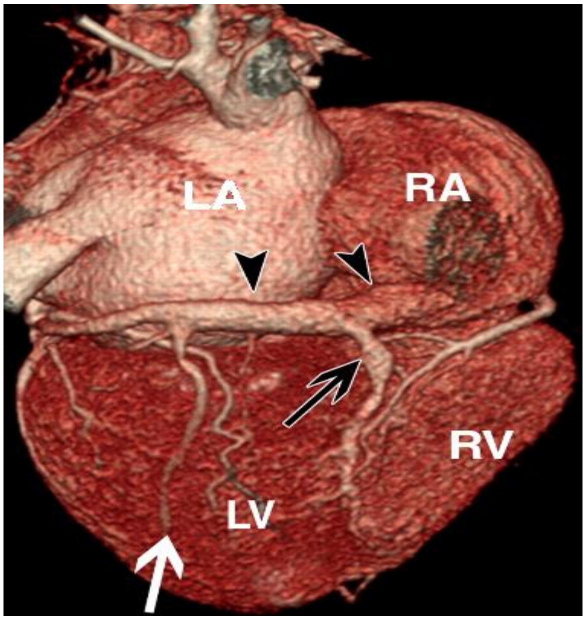

Figure 1.3: Cardiac anatomy

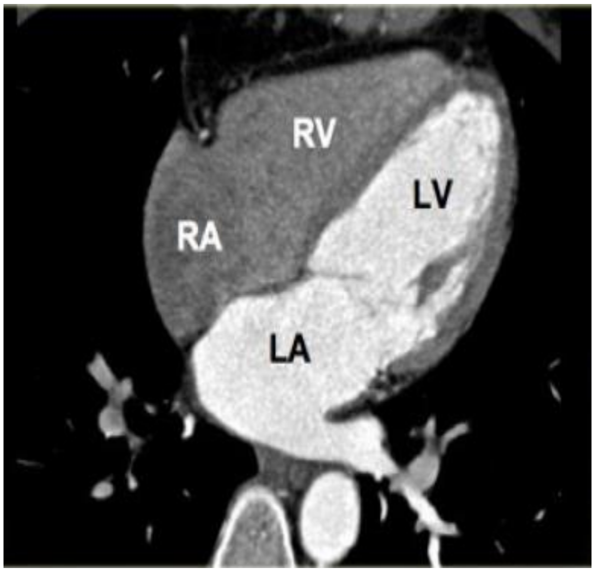

Figure 1.4: Cardiac anatomy in axial slices.

1.2.1 Cardiac Anatomy in 3D MRI

A 3D MRI has various slices in all planes depending upon the temporal resolution of MRI machine. These slice cuts are placed on some non-zero angle, usually 30 degrees. It is due to the fact that human heart is placed at the same angle in the ribcage. Figure 1.5 shows an example of a 3D cut in all planes.

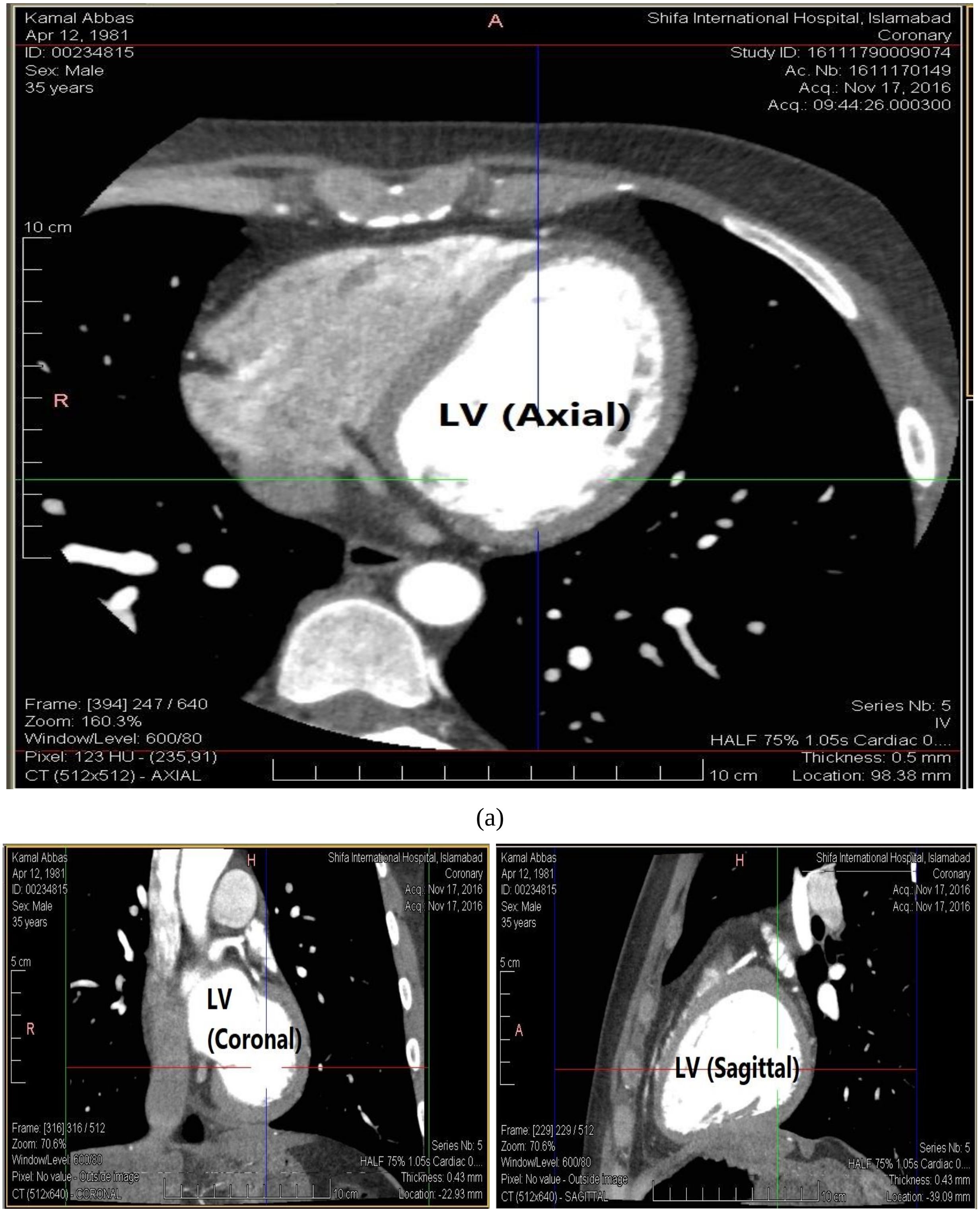

(a)

(b) (c)

Figure 1.5: 290th 3D slice of left ventricle. (a) Axial, (b) Coronal and (c) Sagittal

1.3 Background, Scope and Motivation

Cardiac imaging plays a major role in the diagnostics of various cardio vascular diseases and abnormalities [1-6], such as ventricular tachycardia, atrial fibrillation and myocardial infraction etc. These medical imaging techniques include echo diagram, intravascular ultrasound, 2-D and 3D cardiac MRI, nuclear imaging and CC [7]. Some of these techniques are invasive i.e. use physical catheter which are injected in to a patient body. These physical catheters are painful for patients especially elders and children. Moreover there are patients who have little or non-significant form of disease. Such patients may not require painful invasive techniques. These patients can be dealt with non-invasive techniques like ECHO or MRI. The problem with ECHO cardiograph is that it is based on geometrical assumptions and have poor spatial resolution (see Figure 1.6 for comparison). This technique is getting obsolete. On the other hand modern techniques such as magnetic resonance cardiac imaging has good spatial resolution and provides the necessary information in term of cardiac anatomy. Also MRI techniques are noninvasive. However, magnetic resonance imaging is made difficult by both respiratory motion and cardiac motion occurring at the same time and the poor contrast between adjacent blood pools.

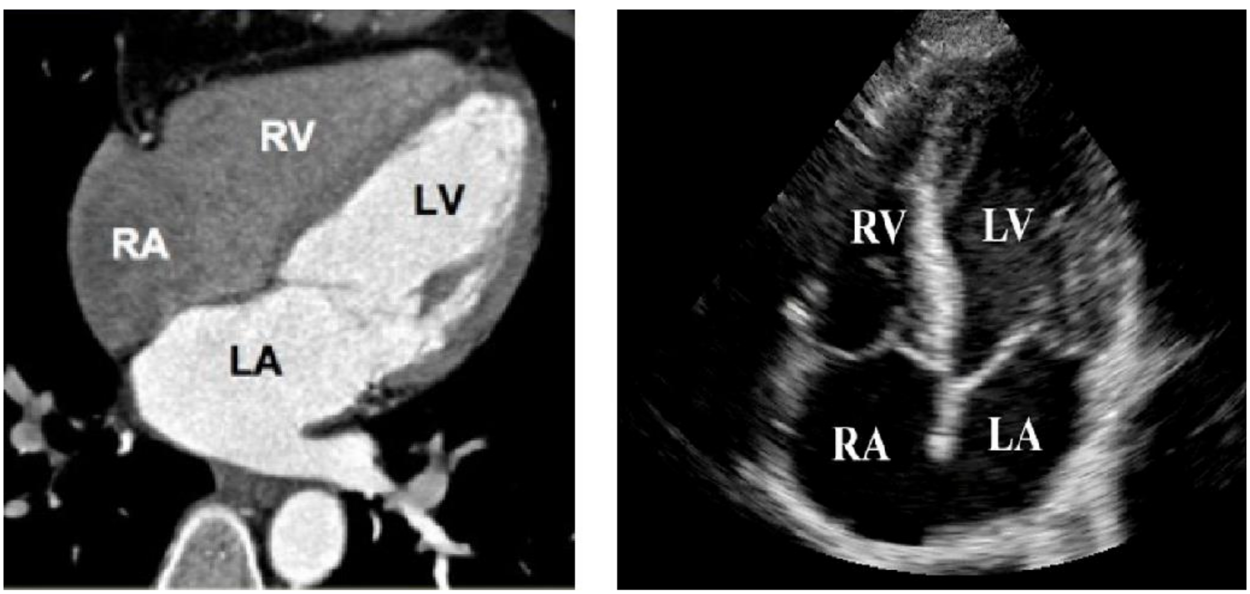

(a) (b)

Figure 1.6: Spatial resolution of (a) MRI and (b) ECHO

Techniques like breath-hold and fast acquisition for 3-D MRI have made drastic improvement to cardiac MRI [8-10]. These techniques have made the diagnostic process more accurate, precise and easy for physicians and patients. However this process still require manual segmentation in order to make raw 3D cardiac MRI readable for physicians. This includes cardiac chamber segmentation (Ventricles and Atrium) and vessels segmentation (includes RCA, LCA, and LAD). For this purpose specific technical and medical training is required to understand and segment raw 3D MRI. The technician also needs to know about the sophisticated post processing softwares. Which means that the pre-diagnosing process depends on the technical skills of the technicians. It is also time consuming for physicians to identify the target anatomy and to perform examination and diagnostics. Therefore it is important for the pre-diagnostic process to have fully automatic segmentation in cardiac images. Although some of the semi-automatic techniques [11-18] have been developed, these methods require some human interaction. Artificial intelligence and fuzzy logic may be used to provide solutions to various image processing and segmentation tasks. [19-21].

This thesis proposes a solution to segment left atrium and left ventricle from 3D MRI images using artificial neural networks in conjunction with traditional image processing approaches. This method identifies and segments the chambers intelligently by an automated system. We then make a 3D segmented model of LA and LV.

Chapter 2 : Literature Review

This chapter provides literature review and basic trends in the field of cardiac chamber (LV and LA) segmentation in 3D MRI. This chapter is divided into three main parts

- Existing techniques
- Comparative analysis of existing techniques
- Complexity analysis of existing techniques.

2.1 Existing Techniques

A few techniques have been developed for cardiac chamber segmentation. These include statistical, shape based morphological, contouring and training approaches [13], [22-27]. The sub sections below presents a detailed overview of some of the existing techniques.

2.1.1 Shape Base Techniques

Shape based techniques take the advantage of the fact that the shape of various objects in a cardiac MRI possess properties of geometrical shapes, such as an ellipse (Figure 2.1), circle or semi cardioid.

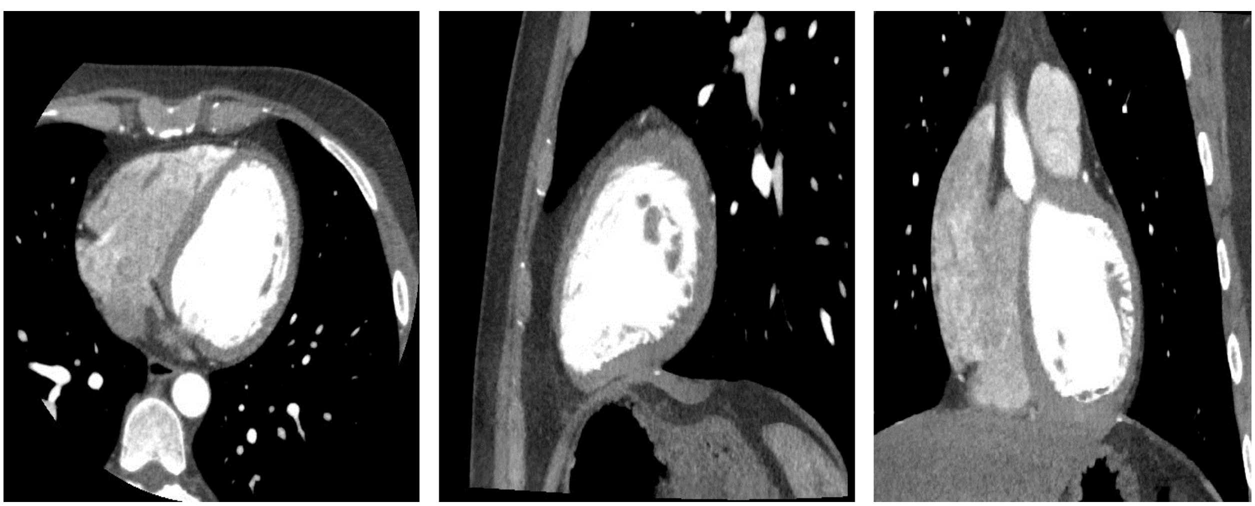

(a) (b) (c)

Figure 2.1: LA shape in (a) Axial (b) Coronal and (c) Sagittal slices.

Shape based methods include bilinear shape based model, variants of Hough transform such as elliptical Hough transform and circular Hough transform etc. Below is the review of some of the common shape based methods.

2.1.1.1 Bilinear Statistical Models

Bilinear shape based model [45], use bilinear statistical models to divide the shape variation into two components i.e. inter-subject variation and intrinsic dynamics of the human heart. This bilinear statistical model is a two-factor model which is linear in any one factor when the other is kept as a constant. With the help of this model it reconstruct the shape of the heart at specific slices in the whole MRI. It however require a small number of shape instances representing the same subject cardiac MRI at different points. This method reconstruct a cardiac model of a maximum 2 mm depth, while the average depth is 3.5 mm.

2.1.1.2 Active Shape Models

An active shape model (ASM) consist of a statistical shape model. This model is known as Point Distribution Model (PDM). It is obtained by a principle component analysis on the set of various aligned shapes Segmentation via ASM is performed by placing the predefined model on the image. And then estimations are rotated iteratively, with different translation and scaling parameters [46]. Due to scaling and translation the shape model is invariant to transformations. The main advantage of the ASM methods is its ability to overcome the noisy structure (which in this case is the non-chamber tissue and ribcage noise). ASM based techniques build a complete shape model using manually segmented data. In ASM a shape model is defined as a structure which reflects the typical structure of a special set of anatomical objects of interest. Variants of ASM may use several ways to represent a shape e.g. cloud point, mesh, surface etc. In most cases for cardiac segmentation, surface and mesh models are mostly used. ASM may have different variants, however the general steps used often are given below.

- contour extraction and spatial alignment
- Temporal alignment
- Construction of the shape model
- Dimensionality reduction
- Shape correspondence

2.1.1.3 Review of Shape Based Methods

However each technique is effective only for specific scenario [28-29]. For example the shape based technique suggested in [17] is appropriate for left ventricle segmentation due to the fact that left ventricle shape resembles ellipse. However this technique fails to segment RA and RV. Similarly [45] is only effective for ventricle segmentation in low resolution MRI. Almost in all cases shape based morphological and contouring methods would not work effectively for all cases due to a high variation and abnormal or irregular cardiac anatomy [22]. To our knowledge, there is no shape based technique reported in the literature for the high resolution (640x512x512 or 0.4mm depth) MRI.

2.1.2 Contours Based Techniques

Previous countering method use the fact that the shape of cardiac chambers remain almost same in subsequent slices [32]. Example of subsequent slices can be seen in figure 2.1 and Figure 2.2, where red arrow point out the LV. A simple approach for chamber segmentation in 3D is to use the manually segmented contours to locate the contour or the boundary in the preceding slice. This type of method can be very effective for chamber segmentation as in each subsequent slices the contours remain almost same. Only the size of the object is changed. So once the chamber is segmented at initial axial slice, it’s not tough to follow it in the preceding slices. However this procedure fails in case of coronal slices, in which the data is not consistent, especially for LV (As shown in Figure 2.2 and Figure 2.3).

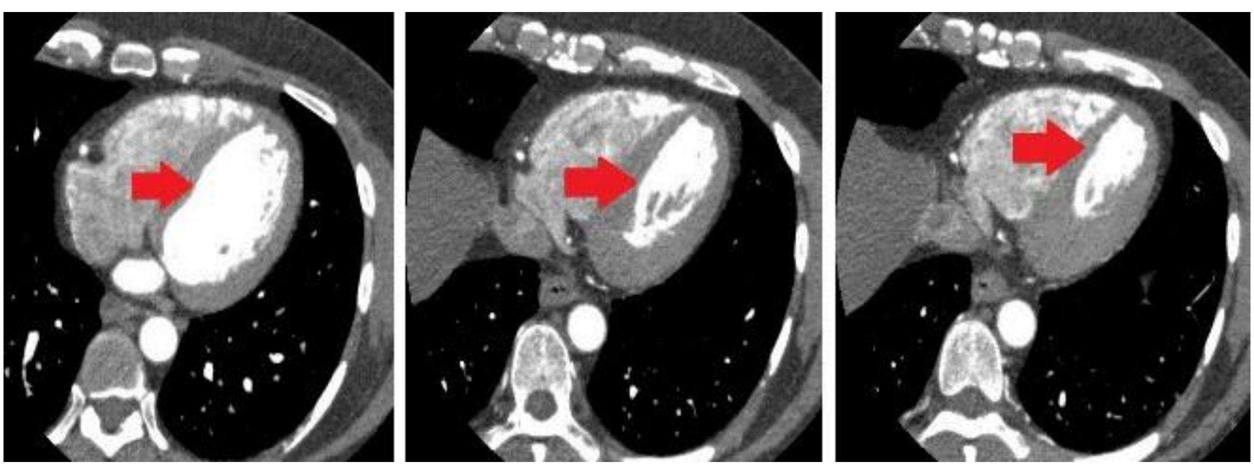

Figure 2.2: Example of consecutive axial slices.

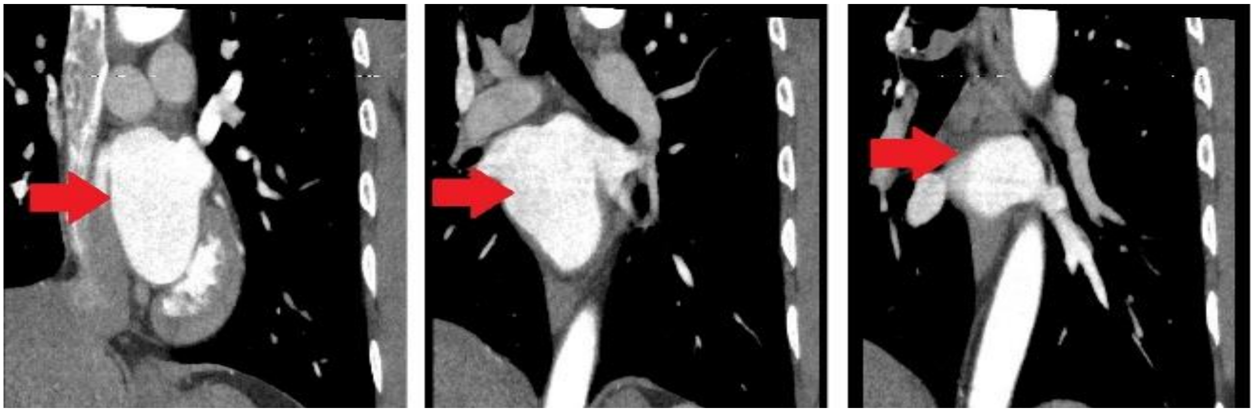

Figure 2.3: Example of consecutive coronal slices.

2.1.2.1 Deformable Models

Deformable models [33-34] or active contours techniques [50-51] are popular model driven technique. It is based on the parametric curves, surfaces or volumes which deforms under various conditions i.e. external and internal energy. The external energy forces the contour to move toward boundary or edge, while the internal energy forces the contour towards smoothness constraint. Adding other energy terms can force the deformable model to achieve better result in case of chamber segmentation. However the biggest disadvantage of this method is that it cannot handle images with more noise. In cardiac images rib cage, backbone and other closely connected vessels act as a noise. Rib cage and backbone can be eliminated but the packed vessels are still a matter of concern for this technique. In 3D MRI as we increase the temporal resolution, the small vessels start appearing prominently in individual slices. Example of noise effect on segmentation can be seen in Figure 2.4.

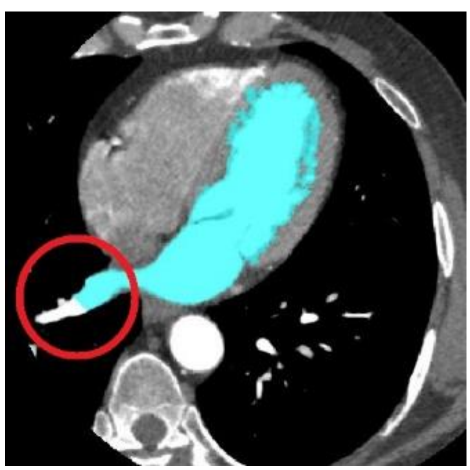

Figure 2.4: Example of a noisy active contour.

The circle in Figure 2.4 shows the segmented vessel. This segmented area is not a part of LA rather it is a part of an artery.

2.1.2.2 Pixel Classification Method

Pixel classification is methods are widely used for medical image segmentation when the dataset have multiple similar images, such as cardiac MRI. In pixel classification methods various features are extracted and are used to classify various objects present in the MRI images. For classification several supervised and unsupervised methods can be used. One of the unsupervised method used in the literature is Gaussian Mixture Model fitting (GMM) and clustering. For this purpose various methods such as geometrical assumptions (LV location, spatial orientation) are used. GMM is based on fitting the image histogram with a combination of various Gaussians using the Expectation-Minimization (EM) algorithm [47].

Until now only a few supervised approaches have been proposed in the literature. It is due to the fact that learning phase is computationally intensive and require a large amount of dataset which is currently not available for high resolution MRI. The learning algorithm is fed with gray levels of labeled MRI pixels. The learning can also be done manually by selecting on a few pixels belonging to LV [48].

2.1.3 Learning Based Estimation Techniques

In learning based shape model, first the cardiac images are manually segmented and then the system is trained with the manually segmented data. Learning based methods in literature are discussed below.

2.1.3.1 Manifold Learning

[30] Uses manifold learning approach based on Mumford-Shah [49] function for shape estimation. Mumford and Shah, proposed a function of the edge set and smooth approximation for segmentation of the input image. It exclude the edge set from the image pixel domain yields a smooth approximation of the input image. The authors manually mark the points for applying shape based mask at start. It that it is not entirely based on AI. Rather it’s a combination of AI and traditional methods. In this work authors have used lesser resolution dataset and the reconstruction is only limited to 2D.

2.1.3.2 Deep Neural Network

To improve learning based method further, deep neural network (DNN) models are identified [31]. With the help of these trained shapes various vessels and LV/RV chambers are segmented. However [31] have not been used for LV and LA pair. Also DNN based methods require large amount of data for training and testing, which in case of cardiac data is not available. Also the available data have a high degree of variability. Less data and high variability may lead to high error rate and inefficient segmentation and reconstruction. However if network is carefully trained with large data, the results may be improved to a high degree. The resulting reconstruction will have high temporal and transversal resolution with highest accuracy. One possible way to tackle this dataset issue is to use other traditional methods along with machine learning techniques such as shallow neural networks.

2.2 Combined Analysis of Existing Methods

From the above review it can be seen that various attempts have been made to segment cardiac chambers. Summary of these methods have been organized in Table 2.1 in detail.

Table 2.1: Comparison of various cardiac chambers segmentation techniques

Ref.	Methodology	Segmentation plane	Automatic / Semi-Automatic	Remarks
[35]	Graph Cuts	2D	Semi-Automatic	
[12]	Seed contour	2D	Semi-Automatic	Issues with discontinuous data
[37]	LARM and ACPS FFDs	3D	Automatic	Computationally intensive. may take hours to complete
[38]	SSDM	2D	Semi-Automatic	Only for Left ventricle segmentation
[13]	Active Shape Model	2D	Automatic	Probabilistic approach having issues with contours. Only for LV

[30]	Phase field approximation, Mumford-Shah functional	3D	Semi-Automatic	Need human interaction at start
[33]	Deformable surface framework	3D	Automatic	Only for Left ventricle segmentation
[17]	Scalable segmentation framework, contour coupling technique	2D	NA	Only for Left ventricle segmentation. Focuses on reducing training effort.
Proposed Method	Neural Networks and traditional methods	3D	Automatic	Less effective for coronal slices of LA

Table 2.1 shows that most of the existing algorithm uses 2D segmentation plane ([12-13][37-38]), i.e. it do not reconstruct a complete 3D model of either left ventricle or left atrium. It can also be seen that most of the existing algorithms are semi-automatic ([30][35][38]), i.e. these techniques need human interaction at some level during segmentation. For example [30] require a manual seed point to be defined at the initial slice. It can also be seen that most of the algorithms ([13][17][33][38]) are applicable to only a single chamber segmentation i.e. LV. These algorithms fail to segment LA due to high variability of LA dataset. In short, without 3D reconstruction the diagnostic process become very difficult. Also semi-automatic algorithms makes the diagnostic more time consuming task.

Table 2.2 shows the segmentation resolution of various existing algorithms in terms of pixels, number of images per MRI sample and millimeters (mm). It can be seen that most of the existing algorithms have lower slices depth or resolution i.e. greater than 1mm in terms of millimeter. It also shows that the existing algorithms are applicable to older MRI techniques having a low transversal and temporal resolution. Such low resolution MRI techniques are unable to reconstruct an accurate 3D model. It can also be seen that the proposed method in this thesis reconstructs LA and LV with the highest resolution.

Table 2.2: Comparison of segmentation resolution of various cardiac chambers segmentation techniques

Ref.	Segmentation Resolution (Pixels)	Segmentation Resolution (No. of images)	Segmentation Resolution (mm)
[12]	256x256	8	10mm
[44]	NA	NA	1.1–2.3mm
[39]	NA	NA	2mm
[30]	120x120	9	NA
[13]	256x256	32	0.93-1.64mm
[37]	280x240	140	1mm
Proposed Algorithm	512x512	512	0.5mm

2.3 Complexity Analysis of Existing Techniques

Table 2.3 shows the complexity analysis of the existing techniques. The complexity is discussed on the basis of computational and mathematical intensity. For example Gaussian filtering is less complex than PCA. PCA is less complex than ASM (Active shape models) and ASM is less complex than LARM and ACPS. The Most complex algorithms are ACM and LARM based such as [37]. According to authors such algorithm may take hours to complete. However there accuracy is better than most of the algorithms. It also have a good temporal resolution of 1mm. It is due to the fact that it construct a 3D model with a slice depth of 140 images per sample. The second most complex algorithms are variants of high order probabilistic estimators [15][11][39]. Their results improve as the order increases, however the complexity is also increased. Such algorithms rely on the tradeoff between accuracy, temporal resolution, transversal resolution and complexity. Learning based estimation methods such as [16] may have less complexity during training. However such techniques are computationally intensive during the training process.

Table 2.3: Detailed complexity analysis of various existing cardiac chamber segmentation techniques

Ref.	Complexity Analysis
[16]	Algorithm is learning based estimation. For 64x64x64 volume at the 3 mm resolution, it requires to calculate $4 * 10^5$ hypothesis, which makes it computationally intensive.
[37]	Based on multiple computationally intensive algorithms i.e. LARM, ACPS and FFDs, According to [34] authors, it may take hours to complete.
[15]	It uses MLP (Maximum likelihood Probability), ellipse fitting, seed countering and thickness estimation with regularized Dirac function.
[11]	Based on high order energy estimation function. Efficiency increases as order increases, however it also increase complexity.
[39]	Based on high order energy estimation function. Efficiency increases as order increases, however it also increase complexity.
[33]	This algorithm is based on ASM (Active Shape model) Construction, Principal Component Analysis and Contour Coupling based objective function.
[17]	Based on ASM (Active Shape model), probabilistic data association filtering (Such as Gaussian filtering) and Mutual Favorite Paring algorithm.
[13]	Based on AAM (Active Appearance model), MPCA (Multilinear Principal component Analysis), probabilistic filtering (Gaussian distribution) and recursive Bayesian framework.
[30]	Estimation based on Mumford-Shah function which is a high order energy estimation function. It requires high computation.
Proposed Method	The algorithm uses a simple 5 layer neural network for junction detection. For tracking and reconstruction it uses connected components algorithm along with Euclidean function.

Chapter 3 : Proposed Methodology

This chapter provides a detailed overview of the proposed method. The chapter is organized in the following parts,

- Introduction
- Proposed algorithm
    - Junction detection
    - Tracking
- Pseudo code

3.1 Introduction

This work targets the segmentation of Left Atrium and Left Ventricle (i.e. LA and LV pair) in high resolution 3D MRI. The proposed method is divided into two major parts i.e. junction detection and LA/LV tracking. The junction detection part is based on AI, where various features are extracted and a neural network is trained with the help of these extracted features to locate the junction between LV and LA. Once the junction is located a traditional tracking methods is used to segment LA and LV. LV is tracked in the subsequent slices and LA in preceding slices. After tracking the segmented layers are stacked above each other to make a 3D segmented model.

The junction detection further consist of training and testing phases. During the first phase neural network is trained for LV and LA junction. Before using neural network some preprocessing is performed. After preprocessing various shape based features are extracted from each objects in the slice. These features are fed into the neural network and after rigorously training the network, it is able to identify the LA/LV junction.

3.2 Proposed Algorithm

The complete framework is shown in Figure 3.1 in the form of a block diagram. MRI slices are first loaded from DICOM data. Then preprocessing is performed and geometric features are extracted. Using these features junction detection is performed on slices using a pre-trained neural network. After junction detection LA and LV are tracked. Finally all the segmented slices are stacked and joined to make a 3D segmented model. Each module of this whole framework is explained in the sub sections below.

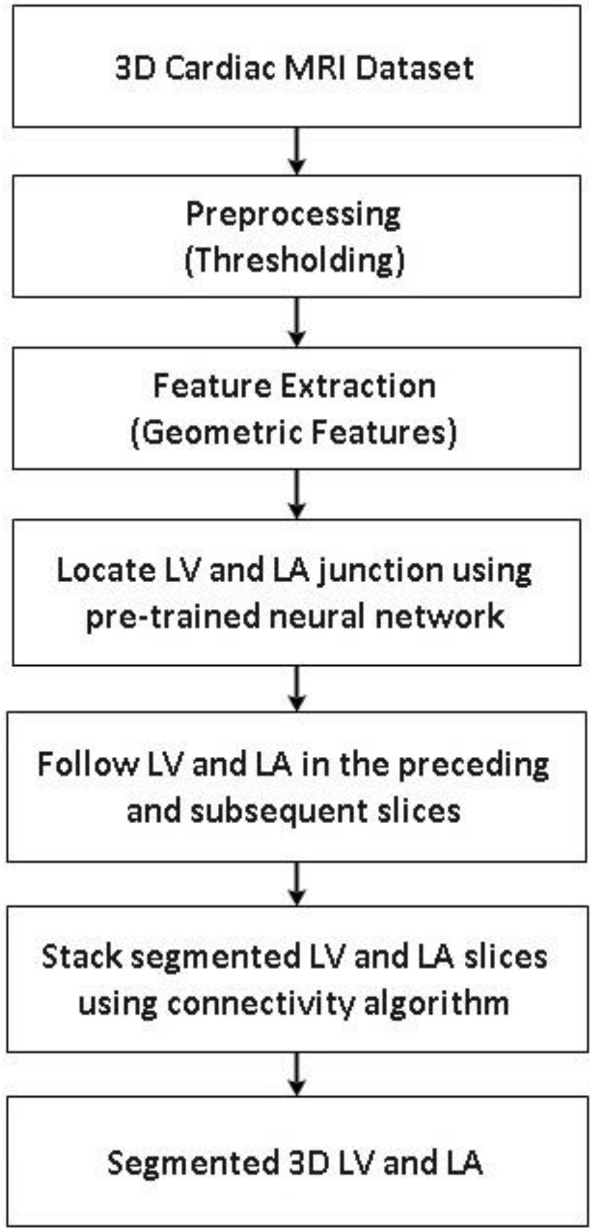

Figure 3.1: Flowchart of proposed framework

3.2.1 Junction Detection

Junction detection is the first step in the proposed cardiac LA and LV segmentation. Figure 3.2 shows the LA and LV, encircled in blue while the red color boundary shows the separation of these two chambers. Figure 3.2 (a) represent LA and LV junction in axial plane, Figure 3.2 (b) represent LA and LV junction in coronal plane while Figure 3.2 (c) represent LA and LV junction in sagittal plane. The steps for junction detection are explained in detailed in the sub sections below.

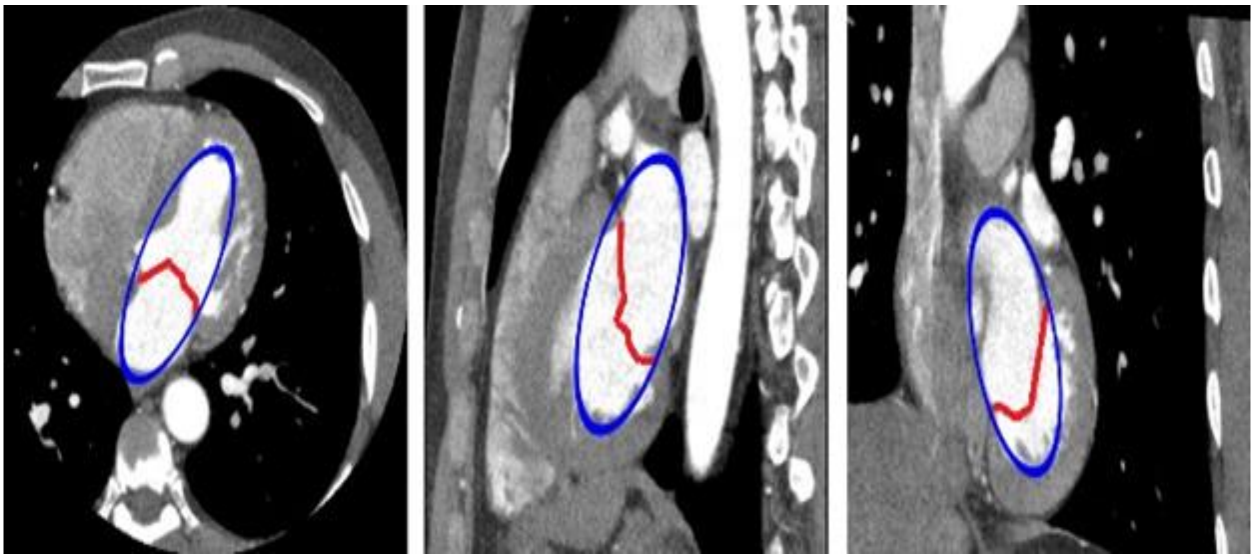

(a) (b) (c)

Figure 3.2: LV and LA junction in (a) Axial (b) Coronal and (c) Sagittal slices.

3.2.1.1 Preprocessing

Pre-processing step includes thresholding of images in all slices in any of the plane. This is done in order to remove noise and prepare the data to extract features for further processing. The noise which need to be removed in this case are the muscular tissues and diluted blood vessels. Some of the noise may still exist in form of bones and parts of arteries which is catered in the feature selection part, where we introduce limit on the area of the objects. Thresholding is done by setting the limit to 85% of the maximum brightness level. This limit has been obtained from vigorous experimentation on various data sets. The 85% threshold provides a good tradeoff between accuracy and effort for feature extraction. Other thresholding methods such as adaptive threshoding and Otsu method do not perform well in this case. Effect of various types of thresholding can be seen in figure 3.3. It can be seen in figure 3.3 that adaptive thresholding fails to negate the tissue of RV and RA. Otsu thresholding also fails to perform. Instead of removing the low contrast noise, it adds it up to the LV.

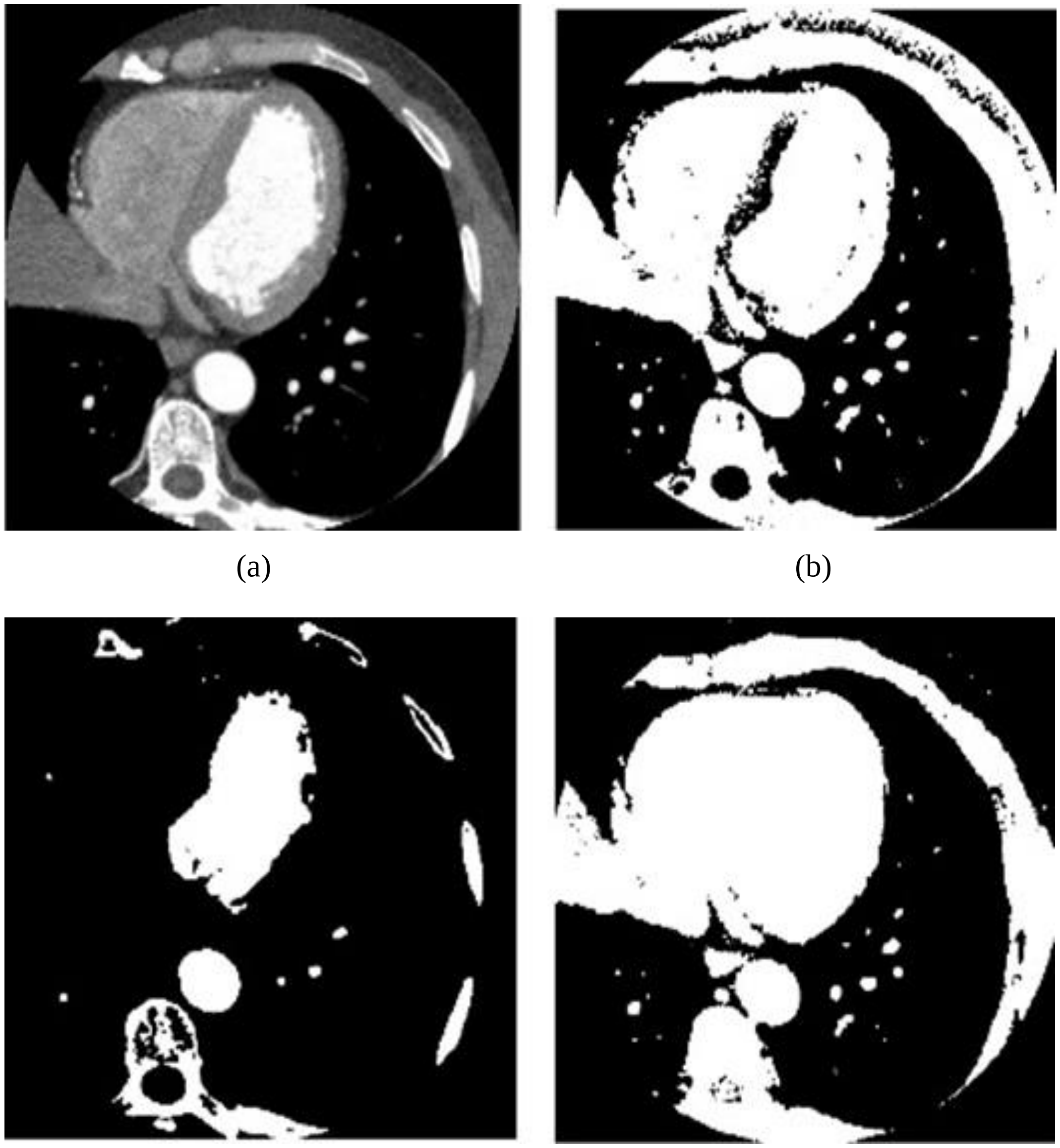

(a) (b) (c) (d)

Figure 3.3: Thresholding (a) Original image (b) Adaptive thresholding (c) Simple thresholding and (d) Otsu thresholding

3.2.1.2 Feature Selection

In figure 3.4 it can be seen that the size of the LA and LV along with its junction is much greater than almost all other objects in all three slices. Analyzing the data set it is observed that the shape of the LV and LA resembles to an ellipse at the junction. Figure 3.4 shows LA and LV junction in red color. The ellipse in blue color shows that they resembles the chamber shape. With the help of this observation some common features can be suggested, which may include parameters related to ellipse, i.e. eccentricity, major axis and area of object (in terms of pixels). Simulations with these features shows that the LA and LV junction can be identified with acceptable accuracy. However our simulations suggests that adding two more features (minor axis and position of object) further improves the segmentation accuracy (Table 3.1). The results shows that using these five features the algorithm becomes more robust towards noise which is caused due to bones and small vessels.

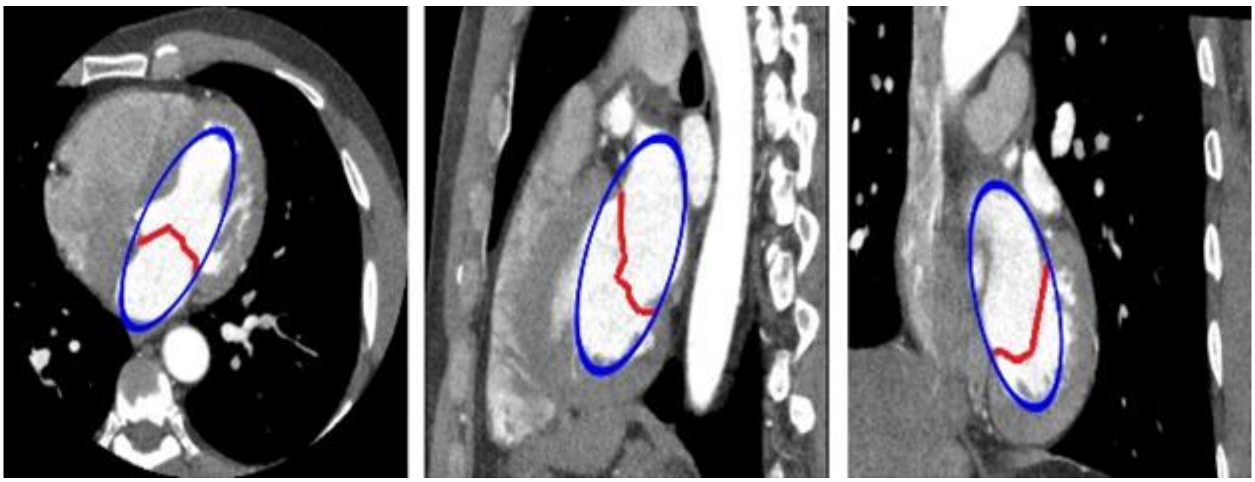

(a) (b) (c)

Figure 3.4: LV and LA junction in (a) Axial (b) Coronal and (c) Sagittal slices.

Table 3.1: Junction detection accuracy based on number of hidden layers

Hidden layers used	**5**	**1**	**3**
Junction Detection Accuracy (Axial)	99.7 %	97.4 %	96.3%
Junction Detection Accuracy (Sagittal)	99.9 %	98.9 %	97.4%
Junction Detection Accuracy (Coronal)	99.9 %	97.4 %	98.3%

3.2.1.3 Feature Extraction

First all objects are detected in a slice by using connectivity algorithm (which is based on connected components algorithms [40] in binary image). The connectivity algorithm performs detection on the binary images which we got from preprocessing phase. The connected component algorithm provides us the list of pixels of individual object in the slice. Using this pixel list all of the five properties of ellipse (area, eccentricity, major axis, minor axis and position) are found for each object in all of the slices. For example for area of individual object we add all the binary pixels of this object. These five features are then used as an input to the neural network.

3.2.1.4 Training the Neural Network

LV and LA junction detection is based on neural network, which uses a simple back propagation algorithm for the training purpose. A sigmoid function is used as an activation function. The network receives five numerical inputs from the feature extraction phase (Figure 3.5). The network provides a single output, either 1 (the object possess a junction) or 0 (this is not the required object).

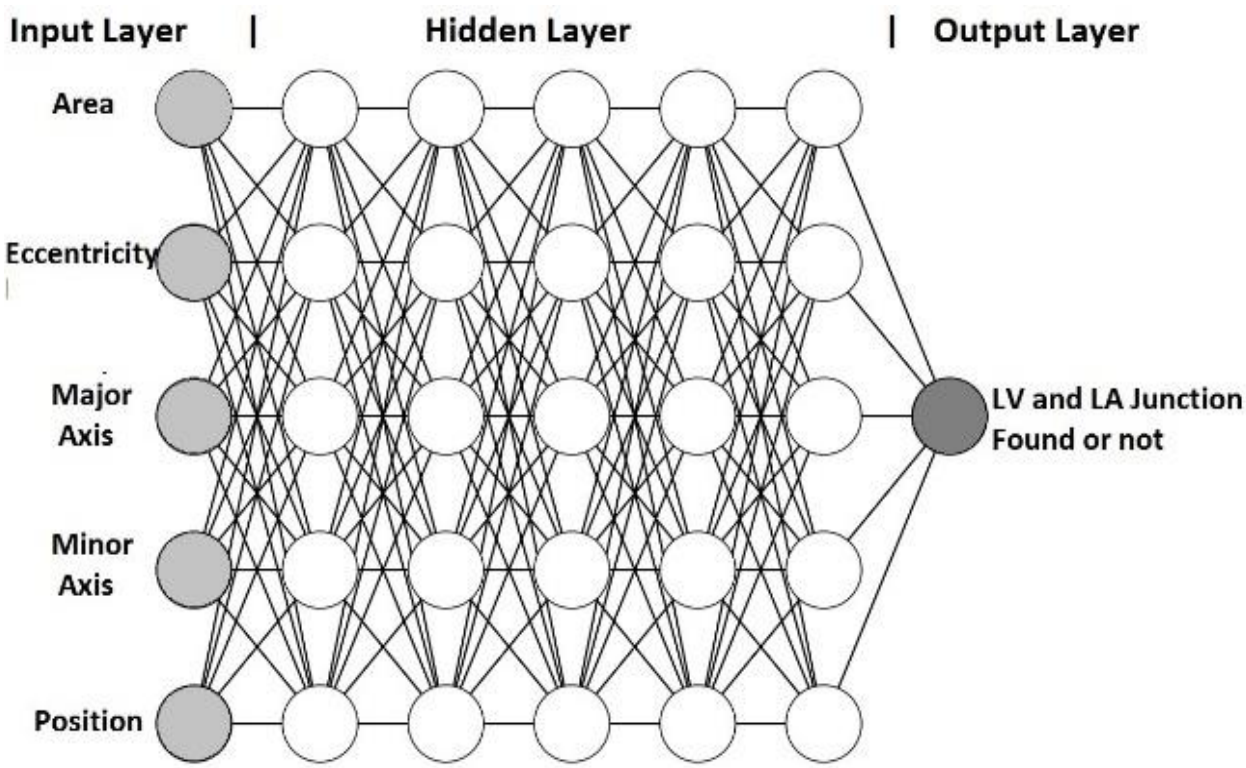

Figure 3.5: Neural network for LA and LV junction detection.

The network is implemented and tested for various hidden layers, where each hidden layer has same number of neurons. It is observed that for five hidden layers with each layer having five neurons, the maximum performance was achieved (Table 3.2)

Table 3.2: Junction detection accuracies based on number of features.

Features used	5	3
Junction Detection Accuracy (Axial)	99.7 %	98.6 %
Junction Detection Accuracy (Sagittal)	99.9 %	97.3 %
Junction Detection Accuracy (Coronal)	99.9 %	97.1 %

3.2.1.5 Testing/Junction Detection

During testing phase similar steps are applied as training. First 3D data is loaded and preprocessing is performed. Then features are extracted from all slices and fed into the trained neural network. The network identifies the slice where the LA and LV junction is present.

3.2.2 Tracking and Construction of 3D Volume

After LA and LV junction is detected, first LV is followed in subsequent slices. For this purpose first slice which is just after the junction is loaded (Figure 3.6). Preprocessing is applied

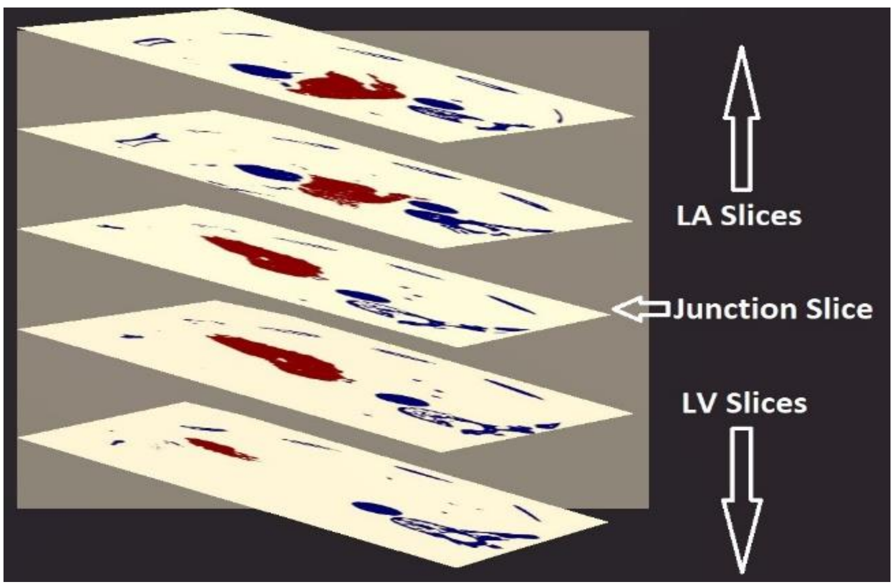

Figure 3.6: 3D slices of segmented images.

to this slice and various objects are detected using connected component algorithm. Now the object which have maximum size and whose center has the minimum Euclidean distance from the junction is declared as LV. After this the next slice is loaded and similar process is followed except that now Euclidean distance is calculated from the previously detected LV. This process continues until the end of LV. In order to detect the end of LV, we set a min threshold on area. If in some slice no object have the area more than the specified threshold, we declare it the end of LV. It is due to the fact that as we move downward, the size of LV gets smaller. Similarly the whole process is repeated for LA, except now we move upward and load preceding slices. After segmentation of LA and LV in all individual slices, all of the segmented slices are simply stacked above each other to generate a 3D segmented shape.

3.3 Pseudo code for LA/LV (Test)

```
1.  Load any of the plane, e.g Axial
2.  Perform preprocessing
3.  Extract features
4.  Detect junction
5.  Load subsequent slices until the end of LV/LA
6.  \IF{Slice number = Junction Slice -1}
7.      Find centers and area of objects detected during
8.      feature extraction
9.      Find euclidean distance between object and junction center
10.     Assign object with min distance and max area as LA/LV.
11. \ELSE
12.     Find centers and area of objects detected during
13.     feature extraction
14.     Find Euclidean distance between object and LA/LV center in preceding slice
15.     Assign object with min distance and max area as LA/LV
16.  \ENDIF
17. \ENDWHILE
18. Stack all the segmented slices
```

Chapter 4 : Experimental Setup and Results

This chapter provides the detailed discussion on the implementation and results of the proposed technique. This chapter is divided into the following parts,

- Experimental Setup
- Results
- Combined Results

4.1 Experimental Setup

The experimental setup consist of the standard data set having total of 21400 high resolution 3D Cardiac MRI images of normal and abnormal human subjects. The dataset is in DICOM format. It contains all three slices, i.e. axial, coronal and sagittal. Further detail of the dataset is given in Table 4.1. The dataset is collected from Shiffa International Hospital. It possess two samples per person. Each sample have 640+512+512 images. The transversal depth of each sample is 0.5mm.

Table 4.1: Dataset details

Data Type	DICOM
Subject Age	28-50
Slices	Axial, Sagittal, Coronal
Depth (Axial)	0.5mm
Depth (Sagittal adf Coronal)	0.43mm
Resolution (Axial)	512x512
Resolution (Sagittal, Coronal)	512x640
No. of Slices (Axial)	640
No. of Slices (Sagittal, Coronal)	512

4.2 Results

Results section has been divided into two parts Junction detection and segmentation. Each of them have been explained in the subsections below.

4.2.1 Junction Detection Results

As stated earlier in neural network subsection, it was found that the five layer neural network showed best performance for junction detection. Figure 4.1 shows training, testing and validation process and their respective error histogram for axial, coronal and sagittal slices. Here the performance of the network is evaluated using cross entropy loss function, which is widely used to measures the performance of a neural network model [41]. Cross entropy increases as the predicted probability of the network diverges from the actual label. For example predicting LA and LV junction with probability of .001 when the actual observation label is 1, would cause a high rate of cross entropy. For an ideal model the cross entropy is always zero. In our case at each epoch the network is trained and cross entropy is calculated. The training and validation process is stopped when minimum cross entropy is achieved in the consecutive epochs. The cross entropy graph in Figure 4.1 shows the min achieved cross entropy for axial, coronal and sagittal slices which is respectively, 0.012502, 0.004408 and 0.00041564 and which was achieved in 28, 32 and 10 epochs respectively. It can be seen that the achieved cross entropy is almost equivalent to zero.

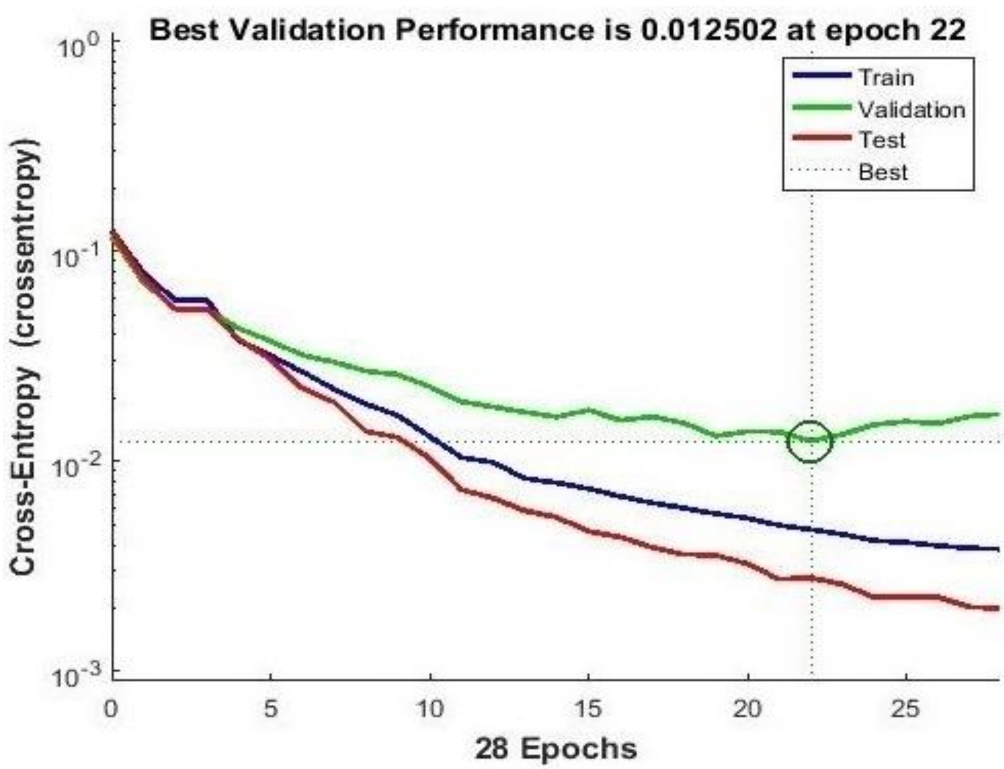

(a)

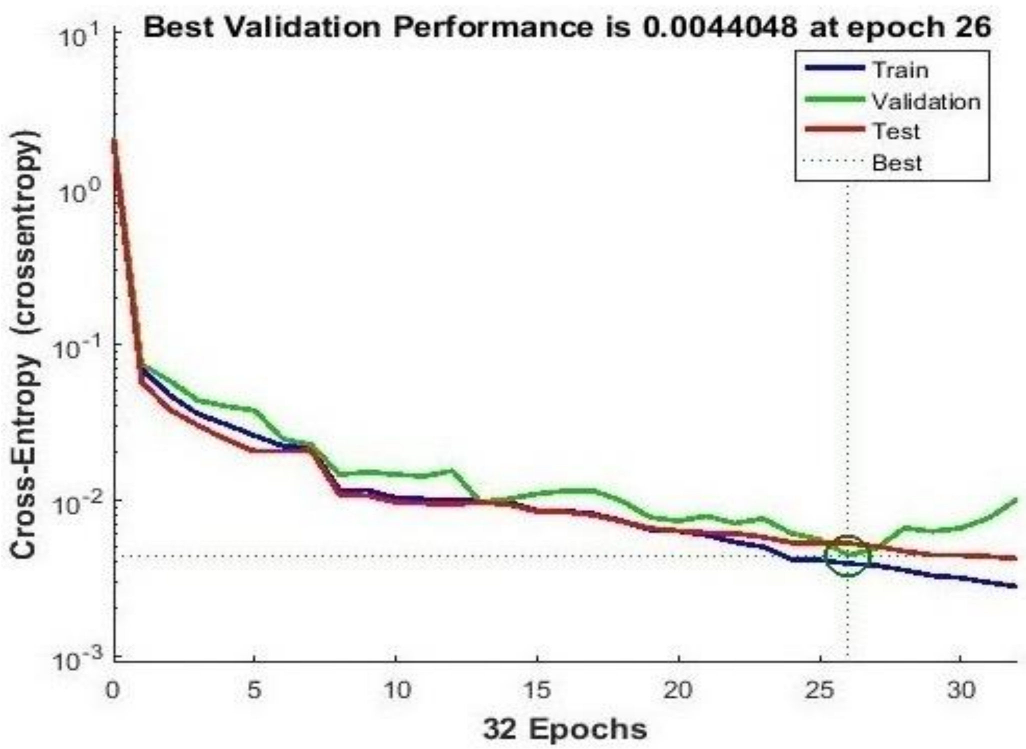

(b)

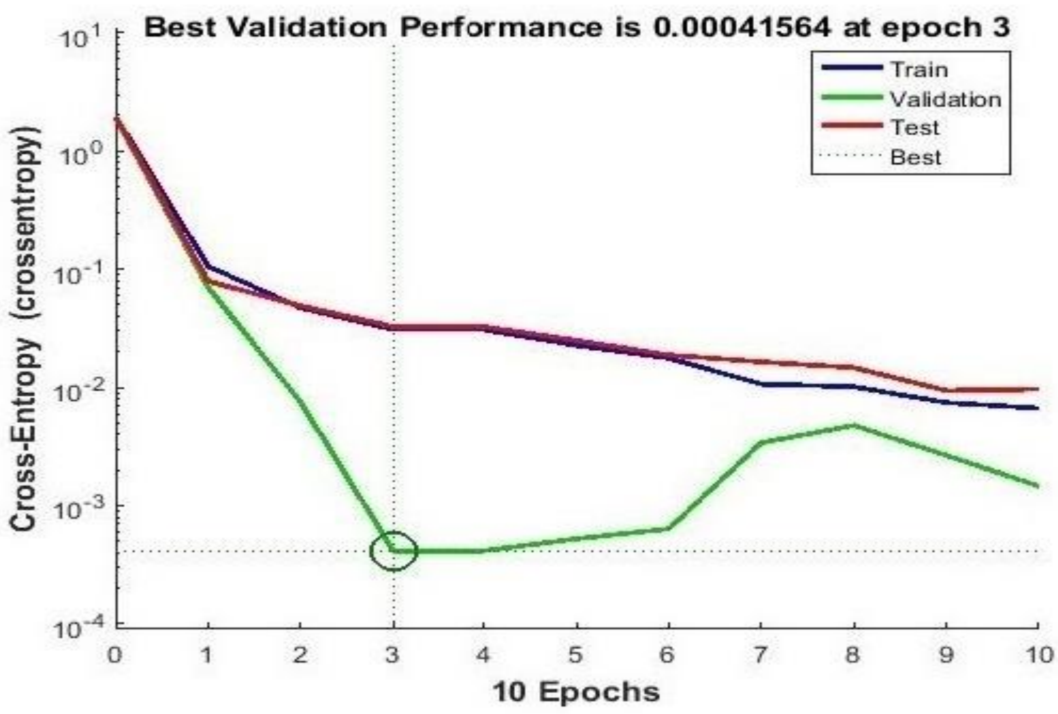

(c)

Figure 4.1: Validation and testing accuracy curves for junction detection in (a) Axial (b) Coronal and (c) Sagittal slices.

The error histogram is also used widely as a performance evaluator in machine learning and artificial intelligence [41]. It classifies the error into various bins. For example the error may be divided into ten discrete levels. Each bin has its own discrete range. Then we draw the histogram for each individual bin based on the error range. The error which has more histogram weight is considered to be more probable. The error histogram shows the maximum possible error that occur during testing phase of a learning algorithm. In our case it can be seen that the combined max error that occurred during training, testing and validation is 0.02306 in axial slices (Figure 4.2 (a)). Figure 4.2 (b) and Figure 4.2 (c) shows respective error histogram for coronal and sagittal slices. The error histogram in Figure 4,2 also shows the number of testing, training and validating instances where this error occurred. The length of blue green and red color in the bar in Figure 4.2 shows training, validation and test error respectively. Note that the error represented in the error histogram is in normalized form. This normalization is in between the range of +1 and -1.

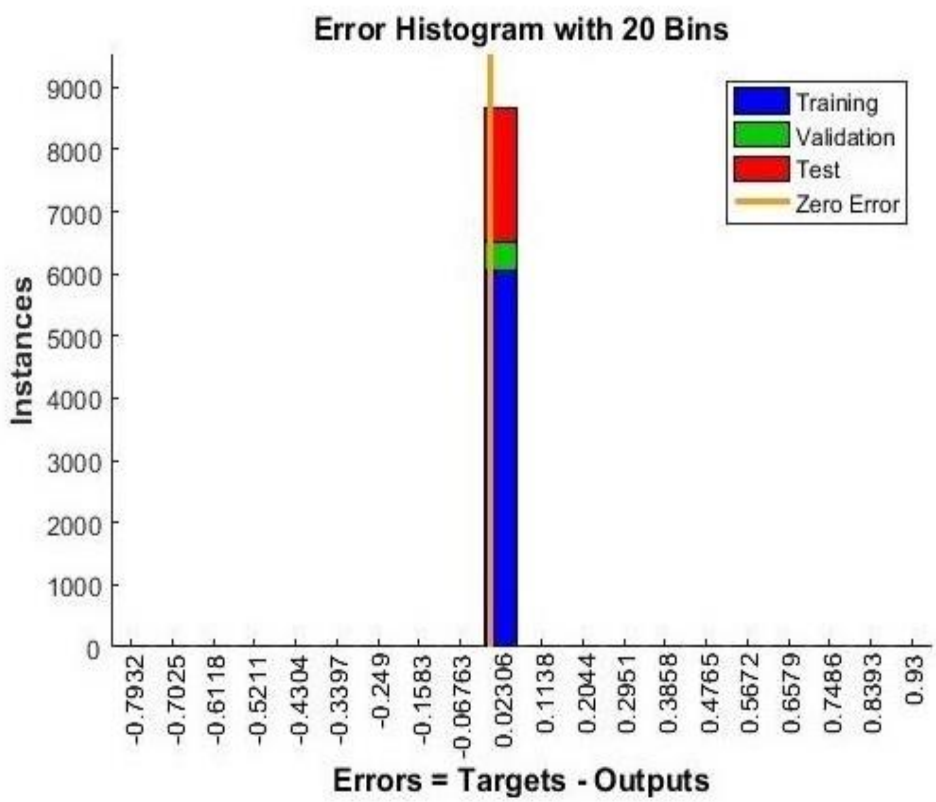

(a)

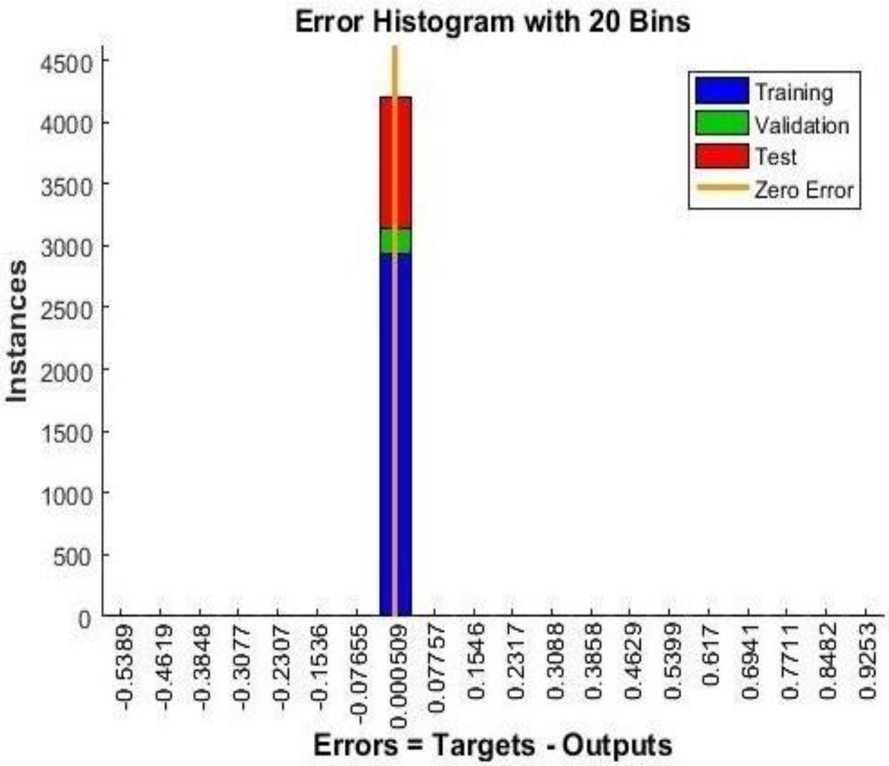

(b)

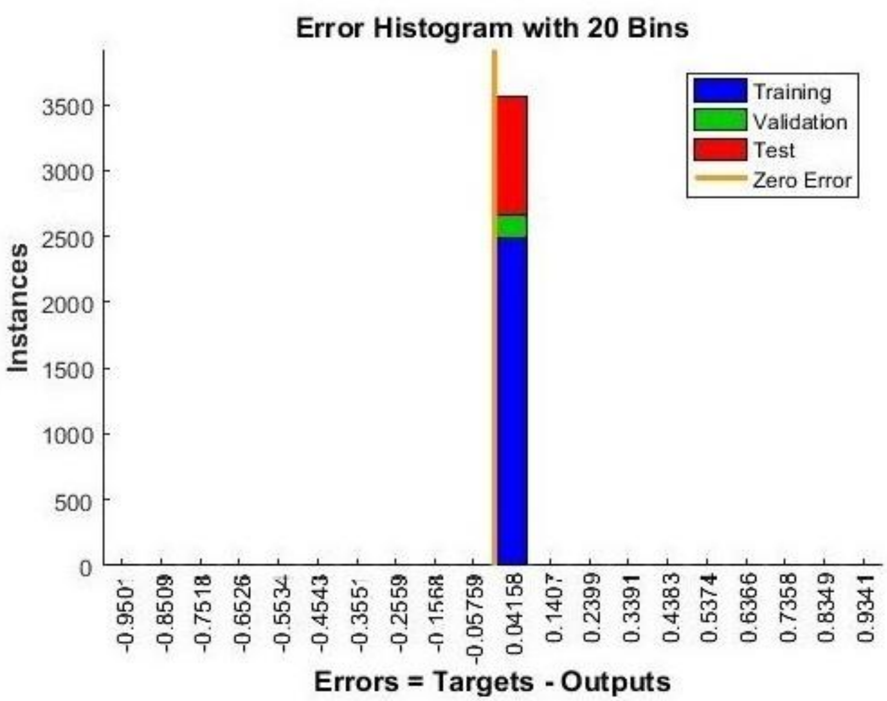

(c)

Figure 4.2: Error histogram for junction detection in (a) Axial, (b) Coronal and (c) Sagittal slices.

4.2.2 Segmentation Results

After junction detection the algorithm is tested for LV and LA segmentation. Figure 4.3 shows some of the results of segmentation in axial plane. Figure 4.31(c) shows the LA and LV junction slice is segmented. Figure 4.3 (a) and (b) show examples of the segmented LA while Figure 4.3 (d) and (f) show examples of the segmented LV. After segmentation all slices are then stacked above each other to generate a complete 3D model of both chambers (Figure 4.4).

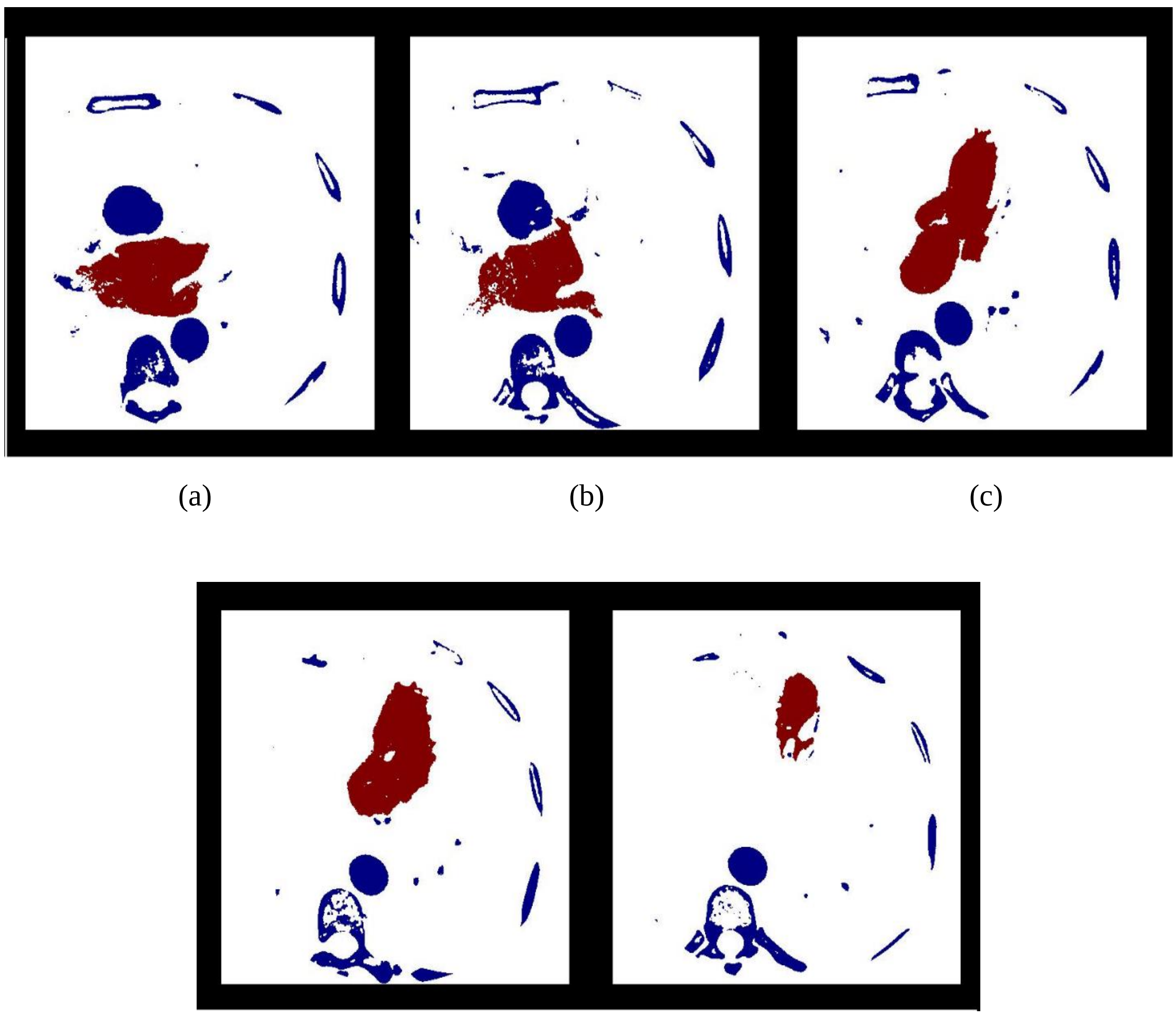

(a) (b) (c)

(d) (e)

Figure 4.3: Simulation results of segmentation in axial slices (a) LA (220^{th} slice) (b) LA (270^{th} slice) (c) Junction of LV and LA is segmented (d) LV (405^{th} slice) and (e) LV (490^{th} slice).

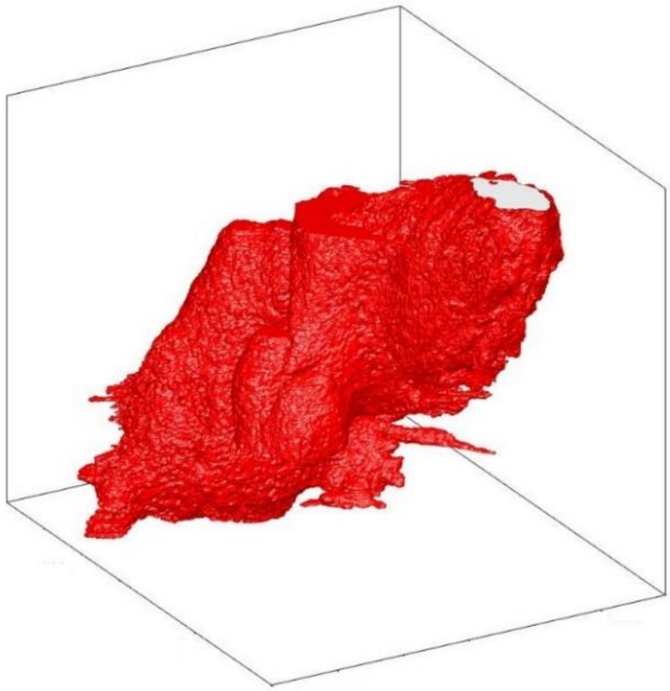

Figure 4.4: 3D reconstruction of LV and LA from segmented slices.

Segmentation results of some of the random slices of axial, coronal and sagittal can be seen in Figure 4.5.

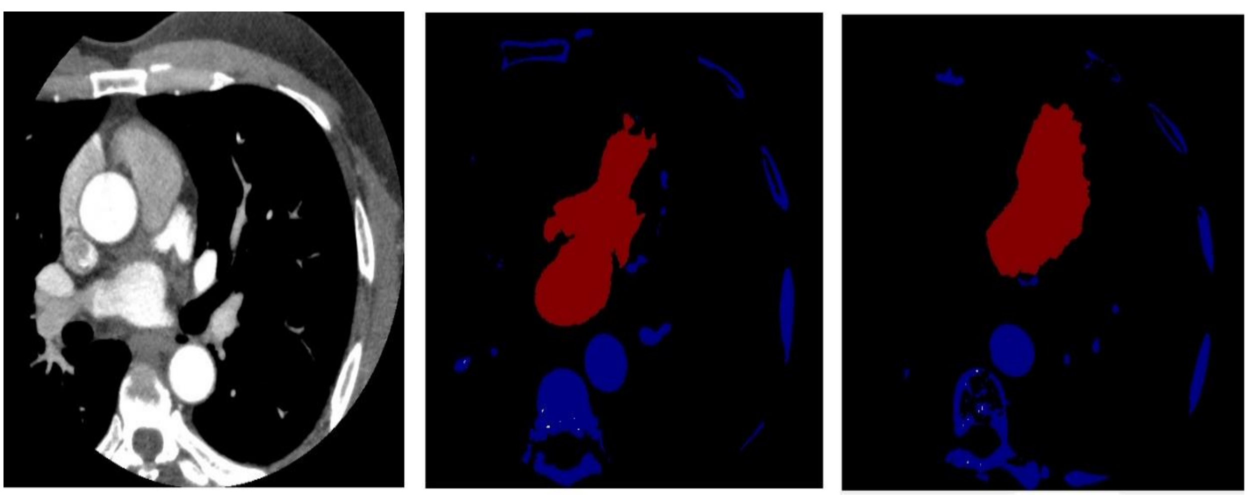

(a) (b) (c)

Figure 4.5: Segmentation results in various random axial slices (a) True negative (b) True positive and (c) True positive

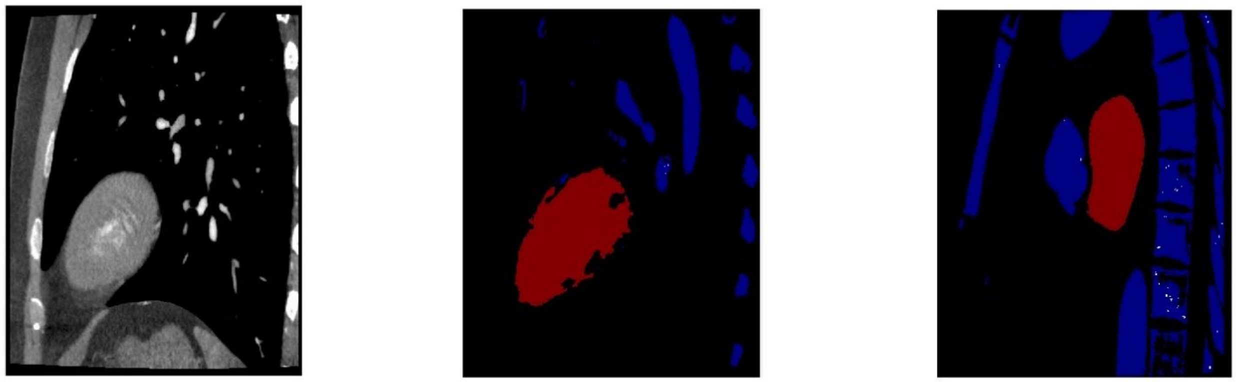

(a) (b) (c)

Figure 4.6: Segmentation results in various random coronal slices (a) True negative (b) True positive and (c) True positive

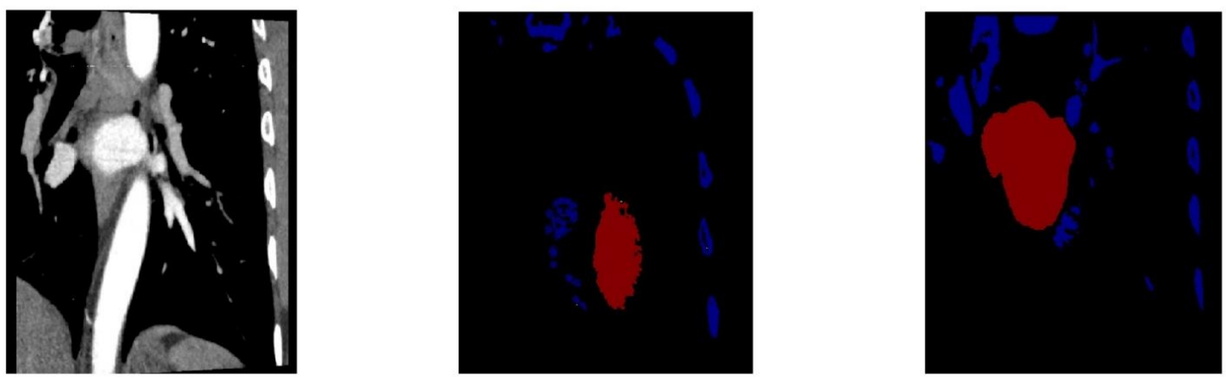

(a) (b) (c)

Figure 4.7: Segmentation results in various random sagittal slices (a) True negative (b) True positive and (c) True positive

All axial slices are compared with the manually segmented model after stacking. During comparison the non-chamber mass (non-chamber tissue such as associated arteries etc.) is measured in terms of pixels. The percentage of non-chamber mass is consider as segmentation error (SE) (Eq. (4.1)). In [37] authors have used mean segmentation error (MSE) as a performance evaluation matrix. The percent inverse of segmentation error is the accuracy (SA). SA can be calculated using Eq. (4.2). The mean of all the accuracies of three slices is known as the mean segmentation accuracy (MSA).

$$SE(\%) = \frac{(Non\ Chamber\ Mass)}{Total\ Mass} * 100 \tag{4.1}$$

where SE is the segmentation error.

$$SA = 100(\%) - SE \tag{4.2}$$

where SA is the segmentation accuracy.

$$MSA = \frac{1}{n}\sum_{i=1}^{n} SA_n \tag{4.3}$$

where n is the number of slices.

The effect of non-chamber mass in individual slices can be seen in Figure 4.8. Figure 4.8 also shows our segmentation accuracy in all three slices. The achieved accuracy for axial slices is 94.4%, for coronal slices the accuracy is 91.71% while for sagittal the accuracy is 88.61%. The overall mean segmentation accuracy is 91.57%.

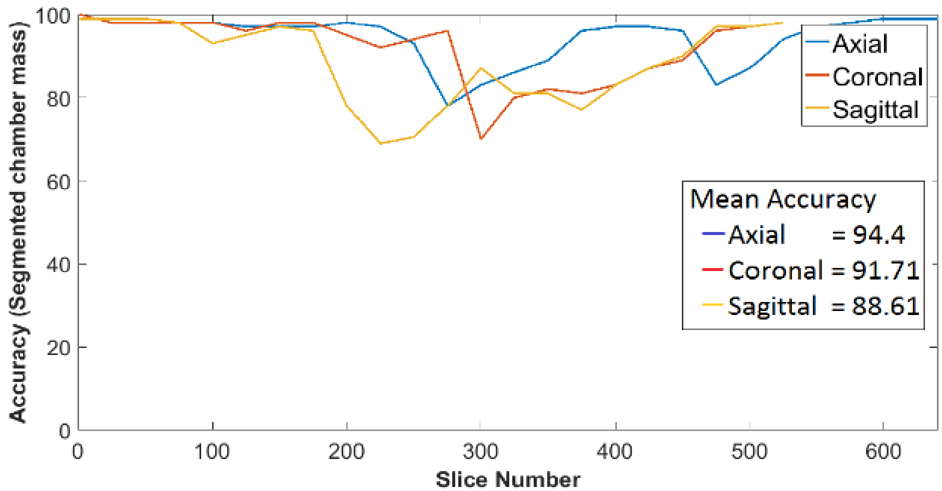

Figure 4.8: Actual chamber mass segmentation in each of the segmented slices (axial, coronal and s agittal).

We have also compared our mean segmentation accuracy with the existing techniques which can be seen in Table 4,2. The results of the proposed method is also validated by computing the dice coefficient (dc) [42], [43], which is widely used for performance evaluation in medical images segmentation. Dice coefficient measures the spatial overlap between manually segmented image (A) and segmented image (B) obtained from the proposed method. Dice coefficient can be found using Eq. (4.4).

$$D_c(A, B) = 2 * \frac{A \cap B}{A + B} \tag{4.4}$$

In our case we find the individual dice coefficient of each slice and then find the average for all of the slices. The results of dice coefficient can be seen in Table 4.2. Table 4.2 shows that the proposed method have the highest dice coefficient as compared to the rest of the techniques. Table 4.2 also shows that the proposed method is far much better than the existing techniques in all aspects. Our technique segment and reconstruct both chambers i.e. LA and LV more accurately.

Table 4.2: Evaluation of our proposed algorithm based on mean square accuracy and dice coefficient.

Ref.	**Chambers Segmented**	**2D/3D Plane**	**3D Reconstruction Done**	**Segmentation Resolution (Pixels, mm)**	**MSA (%)**	d_C
J. Cho [12]	LV and LA	2D axial	No	256x256x8, 10mm	89.3	NA
Lynch et al. [44]	LV	2D axial	No	NA, 1.1–2.3mm	89	NA
Schaerer et al. [39]	LA and LV	2D axial	No	NA, 2mm	NA	91.50
Eslami et al. [30]	LV and LA	2D axial	No	120x120x9, NA	NA	91.54
Santiago et al. [13]	LV	2D axial	No	256x256x32, 0.93-1.64mm	NA	81.1
Zhuang et al. [37]	LV and LA	3D	Yes	280x240x140, 1mm	89.7	86.5
Proposed Algorithm	LV and LA	3D	Yes	512x512x512, 0.5mm	91.57	92.4

4.3 Combined Figurative Results

In Figure 4.9 stepwise figurative results for axial slices can be seen. Figure 4.9 (a) shows original image. Figures 4.9 (b) shows the image after preprocessing step is applied. Figure 4.9 (c) shows the segmented version of the image. Finally Figure 4.9 (d) shows the combined reconstructed 3D segmented LA and LV chambers.

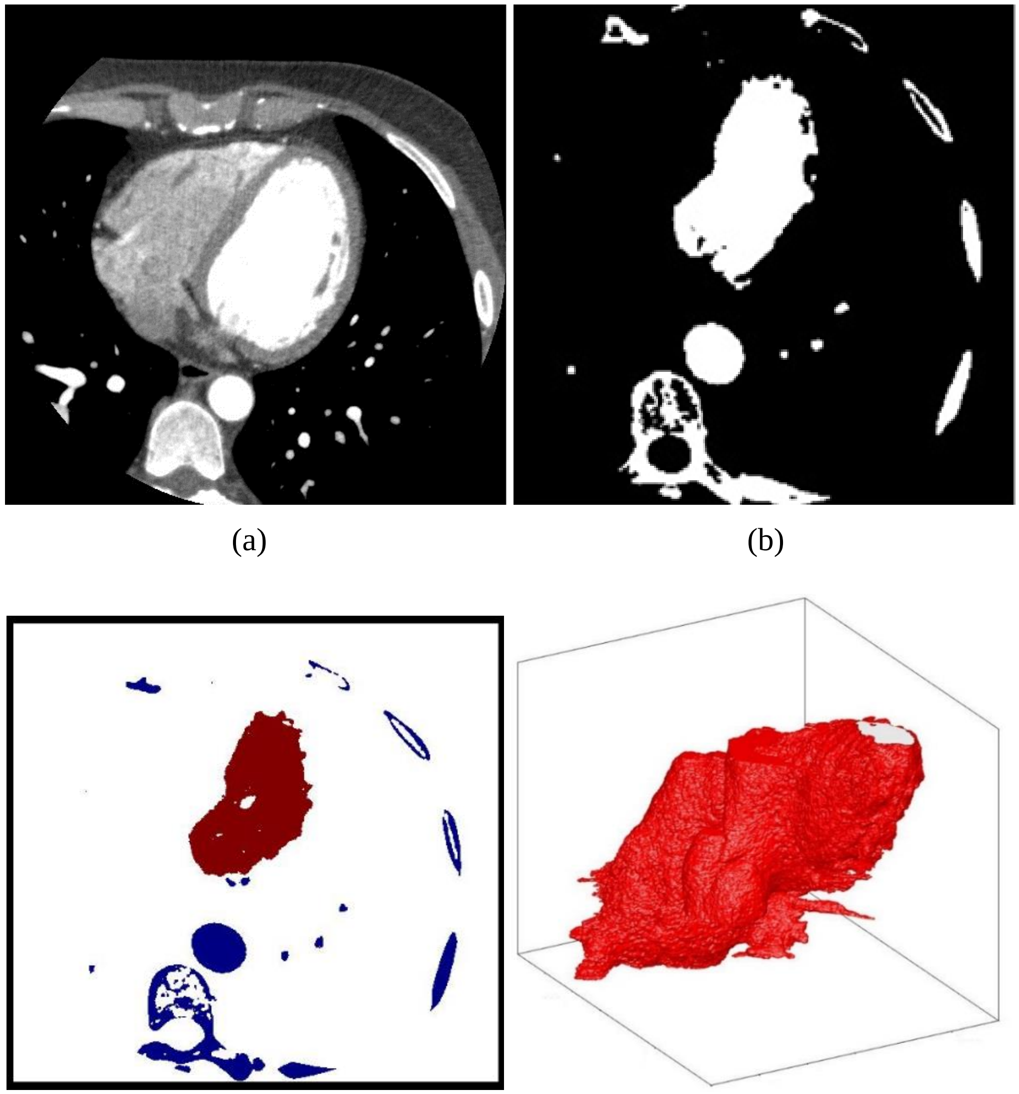

(a) (b)

(c) (d)

Figure 4.9: Step wise results, (a) Original image (b) Preprocessing (c) Segmentation in individual slice and (d) 3D reconstruction

Chapter 5 : Conclusion and Future Work

5.1 Conclusion

In this work a novel technique is proposed to segment cardiac chambers pair i.e. left atrium and left ventricle in a 3D cardiac MRI. This technique uses neural network and other hybrid techniques for cardiac LA and LV chamber segmentation. The technique is divided into two parts i.e. junction detection and tracking. Junction detection is based on object based features, which include size, shape and position. This is due to the fact that the shape of the junction is similar to an ellipse. These features are extracted in the preprocessing process using the connectivity algorithm. These features are fed into a pre trained five layer shallow neural network. The output of the network is either 1 or 0, i.e. either the selected object in the slice possess LA and LV junction or it does not possess the LA and LV junction. After junction detection the LV and LA is tracked in the whole plane using Euclidean function. After tracking all of the slices of LA and LV are sequentially placed and joined to make a complete 3D segmented mass of the LA and LV chambers.

The proposed method is tested on 0.5mm high resolution MRI images dataset. During testing process the proposed algorithm have shown optimum performance in terms of segmentation accuracy. The accuracy is validated using mean segmentation accuracy (MSA) and dice coefficient (Dc), which is widely used as a performance evaluators in image segmentation especially in medical image segmentation. The achieved mean segmentation accuracy is 91.57 while the achieved dice coefficient is 92.4. It is also observed that the proposed technique is fully automatic and independent of the slices depth. This gives the proposed technique an edge over some of the existing techniques, which mostly use manual segmentation at the start. Also the existing algorithms are dependent on slices depth. The proposed technique reconstructs high resolution 3D LA and LV chamber mass. It was also observed that most of the existing algorithms do not reconstruct LA and LV 3D model. The reconstructed resolution is less than 0.5mm in terms of transversal depth, which is the highest resolution reported in the literature.

5.2 Future Work

The proposed technique may be extended to other two chambers (right atrium and right ventricle) which may help to make a complete 3D model of the whole heart. Almost the same algorithm with some modification may be tested for right ventricle and right atrium. RA and RV segmentation may need some more preprocessing along with the proposed method due to more tissue noise..

Other possible approaches can be explored in future which include an implementation of algorithm based completely on deep neural networks. Segmentation of LA and LV based on deep neural networks may be more accurate than the proposed method. However deep neural network based segmentation as for now is not possible due to lack of a large number of standard training dataset. The future work may also include the implementation of right ventricle and right atrium using deep neural network.

REFERENCES

[1] S. H. James, R. Wald, B. J. Wintersperger, L. Jimenez-Juan, D. Deva, M. Crean, E. Nguyen, N. S. Paul, and S. Ley, “Accuracy of right and left ventricular functional assessment by short-axis vs axial cine steady-state free-precession magnetic resonance imaging: intrapatient correlation with main pulmonary artery and ascending aorta phase-contrast flow measurements,” *Canadian Association of Radiologists Journal*, vol. 64, no. 3, pp. 213–219, 2013.

[2] G. Captur, C. Manisty, and J. C. Moon, “Cardiac mri evaluation of myocardial disease,” *Heart*, pp. heartjnl–2015, 2016.

[3] M. Dursun, S. Yılmaz, E. Yılmaz, R. Yılmaz, ˙I. Onur, H. Oflaz, and A. Dindar, “The utility of cardiac mri in diagnosis of infective endo- carditis: preliminary results,” *Diagnostic and Interventional Radiology*, vol. 21, no. 1, p. 28, 2015.

[4] P. Van der Vleuten, T. Willems, M. Go¨tte, R. Tio, M. Greuter, F. Zijlstra, and M. Oudkerk, “Quantification of global left ventricular function: comparison of multidetector computed tomography and magnetic res- onance imaging. a meta-analysis and review of the current literature,” *Acta Radiologica*, vol. 47, no. 10, pp. 1049–1057, 2006.

[5] P. Caro-Dominguez, S.-J. Yoo, M. Seed, and L. Grosse-Wortmann, “Magnetic resonance imaging of cardiovascular thrombi in children,” *Pediatric radiology*, pp. 1–10, 2017.

[6] S. Mehta, S. Panezai, A. Kulhari, A. Z. Arango, L. Suhan, B. DeCar- valho, A. Patel, and J. F. Kirmani, “Abstract wp129: Mri and non-contrast ct clot imaging for successful large vessel clot resolution of posterior circulation ischemic strokes,” 2017.

[7] A. F. Frangi, W. J. Niessen, and M. A. Viergever, “Three-dimensional modeling for functional analysis of cardiac images, a review,” *IEEE Transactions on Medical Imaging*, vol. 20, no. 1, pp. 2–5, Jan 2001.

[8] M. Usman, B. Ruijsink, M. Nazir, G. Cruz, and C. Prieto, “Free breathing whole-heart 3d cine mri with self-gated cartesian trajectory,” *Magnetic Resonance Imaging*, vol. 38, no. Supplement C, pp. 129 – 137, 2017

[9] J. P. Earls, V. B. Ho, T. K. Foo, E. Castillo, and S. D. Flamm, “Cardiac mri: recent progress and continued challenges,” *Journal of magnetic resonance imaging*, vol. 16, no. 2, pp. 111–127, 2002.

[10] W. M. Brink and A. G. Webb, “High permittivity pads reduce specific absorption rate, improve b1 homogeneity, and increase contrast-to-noise ratio for functional cardiac mri at 3 t,” *Magnetic resonance in medicine*, vol. 71, no. 4, pp. 1632–1640, 2014.

[11] M. Hajiaghayi, E. M. Groves, H. Jafarkhani, and A. Kheradvar, “A 3-d active contour method for automated segmentation of the left ventricle from magnetic resonance images,” *IEEE Transactions on Biomedical Engineering*, vol. 64, no. 1, pp. 134–144, Jan 2017.

[12] J. Cho, “Sequential cardiac segmentation by seed contour tracking,” *Electronics Letters*, vol. 40, no. 23, pp. 1467–1469, 2004.

[13] C. Santiago, J. C. Nascimento, and J. S. Marques, “Segmentation of the left ventricle in cardiac mri using a probabilistic data association active shape model,” in 2015 *37th Annual International Conference of the IEEE Engineering in Medicine and Biology Society (EMBC)*, Aug 2015, pp. 7304–7307.

[14] D. Fritz, D. Rinck, R. Unterhinninghofen, R. Dillmann, and M. Scheuer- ing, “Automatic segmentation of the left ventricle and computation of diagnostic parameters using regiongrowing and a statistical model,” in *Medical imaging. International Society for Optics and Photonics*, 2005, pp. 1844–1854.

[15] C. Li, X. Jia, and Y. Sun, “Improved semi-automated segmentation of cardiac CT and MR images,” in Biomedical Imaging: From Nano to Macro, 2009. ISBI’09. *IEEE International Symposium on. IEEE*, 2009, pp. 25– 28.

[16] Y. Zheng, A. Barbu, B. Georgescu, M. Scheuering, and D. Comaniciu, “Four-chamber heart modeling and automatic segmentation for 3-d cardiac CT volumes using marginal space learning and steerable features,” *IEEE Transactions on Medical Imaging*, vol. 27, no. 11, pp. 1668–1681, Nov 2008.

[17] S. P. O’Brien, O. Ghita, and P. F. Whelan, “A novel model-based 3d left ventricular segmentation technique,” *IEEE Transactions on Medical Imaging*, vol. 30, no. 2, pp. 461–474, Feb 2011.

[18] L. Grady, “Random walks for image segmentation,” *IEEE transactions on pattern analysis and machine intelligence*, vol. 28, no. 11, pp. 1768– 1783, 2006.

[19] G. Jeon, M. Anisetti, J. Lee, V. Bellandi, E. Damiani, and J. Jeong, “Concept of linguistic variable-based fuzzy ensemble approach: appli- cation to interlaced hdtv sequences,” *IEEE Trans. Fuzzy Systems*, vol. 17, no. 6, pp. 1245–1258, 2009.

[20] G. Jeon, M. Anisetti, L. Wang, and E. Damiani, “Locally estimated heterogeneity property and its fuzzy filter application for deinterlacing,” *Information Sciences*, vol. 354, pp. 112–130, 2016.

[21] J. Shi, J. Wu, M. Anisetti, E. Damiani, and G. Jeon, “An interval type-2 fuzzy active contour model for auroral oval segmentation,” *Soft Computing*, vol. 21, no. 9, pp. 2325–2345, 2017.

[22] V. Tavakoli and A. A. Amini, “A survey of shaped-based registration and segmentation techniques for cardiac images,” *Computer Vision and Image Understanding*, vol. 117, no. 9, pp. 966–989, 2013.

[23] D. Lesage, E. D. Angelini, I. Bloch, and G. Funka-Lea, “Medial-based bayesian tracking for vascular segmentation: application to coronary arteries in 3d ct angiography,” in Biomedical Imaging: From Nano to Macro, 2008. ISBI 2008. *5th IEEE International Symposium on. IEEE*, 2008, pp. 268–271.

[24] M.-P. Jolly, “Automatic segmentation of the left ventricle in cardiac mr and ct images,” *International Journal of Computer Vision*, vol. 70, no. 2, pp. 151–163, 2006.

[25] H. Tek, Y. Zheng, M. A. Gulsun, and G. Funka-Lea, “An automatic system for segmenting coronary arteries from cta,” *MICCAI-CVII 2011*, pp. 47–54, 2011.

[26] J. Pousin, Y. Rouchdy, M. Picq, J. Schaerer, and P. Clarysse, “Constraint 3d elastic model for the segmentation in cardiac mri,” in *Computers in Cardiology*, 2005. IEEE, 2005, pp. 785–788.

[27] J. Ringenberg, M. Deo, V. Devabhaktuni, O. Berenfeld, B. Snyder, P. Boyers, and J. Gold, “Accurate reconstruction of 3d cardiac geometry from coarsely-sliced mri,” *Computer Methods and Programs in Biomedicine*, vol. 113, no. 2, pp. 483 – 493, 2014.

[28] C. Petitjean and J.-N. Dacher, “A review of segmentation methods in short axis cardiac MR Images,” *Medical image analysis*, vol. 15, no. 2, pp. 169–184, 2011.

[29] S. Ardekani, S. Jain, A. Sanzi, C. P. Corona-Villalobos, T. P. Abraham, M. R. Abraham, S. L. Zimmerman, K. C. Wu, R. L. Winslow, M. I. Miller, and L. Younes, “Shape analysis of hypertrophic and hypertensive heart disease using mri-based 3d surface models of left ventricular geometry,” *Medical Image Analysis*, vol. 29, no. Supplement C, pp. 12 – 23, 2016

[30] A. Eslami, M. Yigitsoy, and N. Navab, “Manifold learning for shape guided segmentation of cardiac boundaries: Application to 3d+ t cardiac mri,” in *Engineering in Medicine and Biology Society, EMBC, 2011 Annual International Conference of the IEEE*. IEEE, 2011, pp. 2658– 2662.

[31] P. V. Tran, “A fully convolutional neural network for cardiac segmenta- tion in short-axis mri,” *arXiv preprint arXiv*: 1604.00494, 2016.

[32] Y. Chenoune, E. Dele´chelle, E. Petit, T. Goissen, J. Garot, and A. Rah- mouni, “Segmentation of cardiac cine-mr images and myocardial de- formation assessment using level set methods,” *Computerized Medical Imaging and Graphics*, vol. 29, no. 8, pp. 607–616, 2005.

[33] J. Montagnat and H. Delingette, “4d deformable models with temporal constraints: application to 4d cardiac image segmentation,” *Medical Image Analysis*, vol. 9, no. 1, pp. 87–100, 2005.

[34] A. Bhan, “Parametric models for segmentation of cardiac mri database with geometrical interpretation,” in *Signal Processing and Integrated Networks (SPIN), 2014 International Conference on. IEEE*, 2014, pp. 711–715.

[35] B. Uzkent, M. J. Hoffman, E. Cherry, and N. Cahill, “3-d mri cardiac segmentation using graph cuts,” in *2014 IEEE Western New York Image and Signal Processing Workshop* (WNYISPW), Nov 2014, pp. 47–51.

[36] U. Kurkure, A. Pednekar, R. Muthupillai, S. D. Flamm, I. A. Kakadiaris et al., “Localization and segmentation of left ventricle in cardiac cine-mr images,” *IEEE transactions on biomedical engineering*, vol. 56, no. 5, pp. 1360–1370, 2009.

[37] X. Zhuang, K. S. Rhode, R. S. Razavi, D. J. Hawkes, and S. Ourselin, “A registration-based propagation framework for automatic whole heart segmentation of cardiac mri,” *IEEE transactions on medical imaging*, vol. 29, no. 9, pp. 1612–1625, 2010.

[38] Y. Zhu, X. Papademetris, A. J. Sinusas, and J. S. Duncan, “Segmentation of the left ventricle from cardiac mr images using a subject-specific dynamical model,” *IEEE Transactions on Medical Imaging*, vol. 29, no. 3, pp. 669–687, 2010.

[39] J. Schaerer, C. Casta, J. Pousin, and P. Clarysse, “A dynamic elastic model for segmentation and tracking of the heart in mr image se- quences,” *Medical Image Analysis*, vol. 14, no. 6, pp. 738–749, 2010.

[40] A. Rosenfeld and J. L. Pfaltz, “Sequential operations in digital picture processing,” *Journal of the ACM* (JACM), vol. 13, no. 4, pp. 471–494, 1966.

[41] L. Alkaiem, F. Keller, and H. Sternberg, “Analysis of inclination measurement by means of artificial neural networks–a comparison of static and dynamic networks.”

[42] M. Lynch, O. Ghita, and P. F. Whelan, “Segmentation of the left ventricle of the heart in 3D MRI data using an optimized nonrigid temporal model,” *IEEE Transactions on Medical Imaging*, vol. 27, no. 2, pp. 195–203, 2008.

[43] L. R. Dice, “Measures of the amount of ecologic association between species,” *Ecology*, vol. 26, no. 3, pp. 297–302, 1945.

[44] M. Lynch, O. Ghita, and P. F. Whelan, “Left-ventricle myocardium segmentation using a coupled level-set with a priori knowledge,” *Com- puterized Medical Imaging and Graphics*, vol. 30, no. 4, pp. 255–262, 2006.

[45] Hoogendoorn, Corné, et al. "Bilinear models for spatio-temporal point distribution analysis." *International Journal of Computer Vision* 85.3 (2009): 237-252.

[46] Cootes, T., Cooper, D., Taylor, C., Graham, J., 1995. Active shape models – their training and application. *Comput. Vis. Image Understand*. 61 (1), 38–59.

[47] Dempster, A., Laird, N., Rubin, D., 1977. Maximum likelihood from incomplete data via the EM algorithm. J. Roy. Stat. Soc. 39 (1), 1–38.

[48] Stalidis, G., Maglaveras, N., Efstratiadis, S., Dimitriadis, A., Pappas, C., 2002. Modelbased processing scheme for quantitative 4-D cardiac MRI analysis. *IEEE Trans. Inf. Technol. Biomed*. 6 (1), 59–72.

[49] D. Mumford, J. Shah, "Optimal Approximation by Piecewise Smooth Functions and Associated Variational Problems," *Comm. Pure* Appl. Math., vol. 42, p. 577–685, 1989.

[50] M. Kass, A. Witkin, D. Terzopoulos, Snakes: Active contour models, Int. J. *Comput. Vis.* 1 (4) (1988) 321–331.

[51] C. Metz, S. Klein, M. Schaap, T. van Walsum, W. Niessen, Nonrigid registration of dynamic medical imaging data using nD+T B-splines and a groupwise optimization approach, *Med. Image Anal*. 15 (2) (2011) 238–249.

[52] Alexander J. ED, Iaizzo, Paul A. 2015, Attitudinally Correct Cardiac Anatomy, Handbook of Cardiac Anatomy, Physiology, and Devices, Springer International Publishing, https://doi.org/10.1007/978-3-319-19464-6_2, 10.1007/978-3-319-19464-6_2